[34] A. du Bois, H.J. Luck, W. Meier, H.P. Adams, V. Mobus, S. Costa, T. Bauknecht, B. Richter, M. Warm, W. Schroder, S. Olbricht, U. Nitz, C. Jackisch, G. Emons, U. Wagner, W. Kuhn, J. Pfisterer, A randomized clinical trial of cisplatin/paclitaxel versus carboplatin/paclitaxel as first-line treatment of ovarian cancer, J. Natl. Cancer Inst. 95 (2003) 1320–1329.
[35] J. Cassidy, J. Tabernero, C. Twelves, R. Brunet, C. Butts, T. Conroy, F. Debraud, A. Figer, J. Grossmann, N. Sawada, P. Schoffski, A. Sobrero, E. Van Cutsem, E. Diaz-Rubio, XELOX (capecitabine plus oxaliplatin): active first-line therapy for patients with metastatic colorectal cancer, J. Clin. Oncol. 22 (2004) 2084–2091.
[36] A. Horwich, D.T. Sleijfer, S.D. Fossa, S.B. Kaye, R.T. Oliver, M.H. Cullen, G.M. Mead, R. de Wit, P.H. de Mulder, D.P. Dearnaley, P.A. Cook, R.J. Sylvester, S.P. Stenning, Randomized trial of bleomycin, etoposide, and cisplatin compared with bleomycin, etoposide, and carboplatin in good-prognosis metastatic nonseminomatous germ cell cancer: a Multiinstitutional Medical Research Council/European Organization for Research and Treatment of Cancer Trial, J. Clin. Oncol. 15 (1997) 1844–1852.
[37] J. Bellmunt, A. Ribas, N. Eres, J. Albanell, C. Almanza, B. Bermejo, L.A. Sole, J. Baselga, Carboplatin-based versus cisplatin-based chemotherapy in the treatment of surgically incurable advanced bladder carcinoma, Cancer 80 (1997) 1966–1972.
[38] N. Nishiyama, S. Okazaki, H. Cabral, M. Miyamoto, Y. Kato, Y. Sugiyama, K. Nishio, Y. Matsumura, K. Kataoka, Novel cisplatin-incorporated polymeric micelles can eradicate solid tumors in mice, Cancer Res. 63 (2003) 8977–8983.
[39] H. Uchino, Y. Matsumura, T. Negishi, F. Koizumi, T. Hayashi, T. Honda, et al., Cisplatin-incorporating polymeric micelles (NC-6004) can reduce nephrotoxicity and neurotoxicity of cisplatin in rats, Br. J. Cancer 93 (2005) 678–687.
[40] L.H. Li, T.J. Fraser, E.J. Olin, B.K. Bhuyan, Action of camptothecin on mammalian cells in culture, Cancer Res. 32 (1972) 2643–2650.
[41] R.C. Gallo, J. Whang-Peng, R.H. Adamson, Studies on the antitumor activity, mechanism of action, and cell cycle effects of camptothecin, J. Natl. Cancer Inst. 46 (1971) 789–795.
[42] J.A. Gottlieb, A.M. Guarino, J.B. Call, V.T. Oliverio, J.B. Block, Preliminary pharmacologic and clinical evaluation of camptothecin sodium (NSC-100880), Cancer Chemother. Rep. 54 (1970) 461–470.
[43] F.M. Muggia, P.J. Creaven, H.H. Hansen, M.H. Cohen, O.S. Selawry, Phase I clinical trial of weekly and daily treatment with camptothecin (NSC-100880): correlation with preclinical studies, Cancer Chemother. Rep. 56 (1972) 515–521.
[44] D. Cunningham, S. Pyrhonen, R.D. James, C.J. Punt, T.F. Hickish, R. Heikkila, et al., Randomised trial of irinotecan plus supportive care versus supportive care alone after fluorouracil failure for patients with metastatic colorectal cancer, Lancet 352 (1998) 1413–1418.
[45] L.B. Saltz, J.V. Cox, C. Blanke, L.S. Rosen, L. Fehrenbacher, M.J. Moore, et al., Irinotecan plus fluorouracil and leucovorin for metastatic colorectal cancer. Irinotecan Study Group, N. Engl. J. Med. 343 (2000) 905–914.
[46] K. Noda, Y. Nishiwaki, M. Kawahara, S. Negoro, T. Sugiura, A. Yokoyama, et al., Irinotecan plus cisplatin compared with etoposide plus cisplatin for extensive small-cell lung cancer, N. Engl. J. Med. 346 (2002) 85–91.
[47] S. Negoro, N. Masuda, Y. Takada, T. Sugiura, S. Kudoh, N. Katakami, et al., CPT-11 Lung Cancer Study Group West. Randomised phase III trial of irinotecan combined with cisplatin for advanced non-small-cell lung cancer, Br. J. Cancer 88 (2003) 335–341.
[48] D.C. Bodurka, C. Levenback, J.K. Wolf, J. Gano, J.T. Wharton, J.J. Kavanagh, et al., Phase II trial of irinotecan in patients with metastatic epithelial ovarian cancer or peritoneal cancer, J. Clin. Oncol. 21 (2003) 291–297.
[49] C.H. Takimoto, S.G. Arbuck, Topoisomerase I targeting agents: the camptothecins, in: B.A. Chabner, DL Lango (Eds.), Cancer Chemotherapy and Biotherapy: Principal and Practice, 3rd ed, Lippincott Williams & Wilkins, Philadelphia (PA), 2001, pp. 579–646.
[50] J.G. Slatter, L.J. Schaaf, J.P. Sams, K.L. Feenstra, M.G. Johnson, P.A. Bombardt, et al., Pharmacokinetics, metabolism, and excretion of irinotecan (CPT-11) following I.V. infusion of [(14)C]CPT-11 in cancer patients, Drug Metab. Dispos. 28 (2000) 423–433.
[51] M.L. Rothenberg, J.G. Kuhn, H.A. Burris 3rd, J. Nelson, J.R. Eckardt, M. Tristan-Morales, et al., Phase I and pharmacokinetic trial of weekly CPT-11, J. Clin. Oncol. 11 (1993) 2194–2204.
[52] S. Guichard, C. Terret, I. Hennebelle, I. Lochon, P. Chevreau, E. Fretigny, et al., CPT-11 converting carboxylesterase and topoisomerase activities in tumor and normal colon and liver tissues, Br. J. Cancer 80 (1999) 364–370.
[53] M. Yokoyama, T. Okano, Y. Sakurai, H. Ekimoto, C. Shibazaki, K. Kataoka, Toxicity and antitumor activity against solid tumors of micelle-forming polymeric anticancer drug and its extremely long circulation in blood, Cancer Res. 51 (1991) 3229–3236.
[54] L.B. Saltz, J.Y. Douillard, N. Pirotta, et al., Irinotecan plus fluorouracil/leucovorin for metastatic colorectal cancer: a new survival standard, Oncologist 6 (2001) 81–91.
[55] J.Y. Douillard, D. Cunningham, A.D. Roth, et al., Irinotecan combined with fluorouracil compared with fluorouracil alone as first-line treatment for metastatic colorectal cancer: a multicentre randomised trial, Lancet 355 (2000) 1041–1047.
[56] F. Koizumi, M. Kitagawa, T. Negishi, et al., Novel SN-38-incorporating polymeric micelles, NK012, eradicate vascular endothelial growth factor-secreting bulky tumors, Cancer Res. 66 (2006) 10048–10056.
[57] T. Eguchi Nakajima, M. Yasunaga, Y. Kano, K. Shirao, Y. Shimada, Y. Matsumura, Synergistic antitumour activity of the novel SN-38-incorporating polymeric micelles, NK012, combined with 5-fluorouracil in a mouse model of colorectal cancer, as compared with that of irinotecan plus 5-fluorouracil, Int. J. Cancer. 122 (2008) 2148–2153.

Loss of heterozygosity of the PTH/PTHrP type 1 receptor in oral squamous cell carcinoma

HITOSHI MIYASHITA[1], SHIRO MORI[1], YUTAKA FUKUMOTO[3], ATUSHI SATO[4], MANABU FUKUMOTO[2] and HIROSHI KAWAMURA[1]

[1]Division of Maxillofacial Surgery, Department of Oral Medicine and Surgery, Graduate School of Dentistry, and [2]Department of Pathology, Institute of Development, Aging and Cancer, Tohoku University, Sendai 980-8575; [3]Department of Oral Surgery, Tokyo Metropolitan Futyu Hospital, Tokyo 183-8524; [4]Department of Oral Surgery, Sendai Medical Center, Sendai 983-8520, Japan

Received June 12, 2008; Accepted July 25, 2008

DOI: 10.3892/mmr_00000034

Abstract. Parathyroid hormone-related protein (PTHrP) is produced by various types of carcinomas, and is an important factor in the development of bone metastasis. The coexpression of PTHrP and parathyroid hormone/parathyroid hormone-related protein type 1 receptor (PTHR1) in cancer predicts poor patient survival. While genetic transformations of thyroid hormone receptor ß (THRß) have been reported as being associated with reduced survival in patients with oral squamous cell carcinoma (OSCC), the details of transformations in PTHR1 have not been extensively analyzed. The aim of this study was to examine loss of heterozygosity (LOH) and microsatellite instability (MSI) in PTHR1 in OSCC. Analysis of genetic transformations using microdissected clinical tissues revealed that the proportions of LOH and MSI in PTHR1 were 30.0 (3/10) and 20.0% (2/10), respectively. Furthermore, the proportion of carcinomas which developed with LOH on the chromosome of PTHR1 and without LOH for tumor suppressor genes such as *p53*, *FHIT*, *APC*, *BRCA1*, *BRCA2* and *DCC* was 20.0% (2/10). These observations suggest that transformations in PTHR1 may be involved in carcinogenesis in human OSCC.

Introduction

Parathyroid hormone-related protein (PTHrP) is in part responsible for the clinical syndrome termed humoral hypercalcemia of malignancy (HHM), and has been implicated as an important factor in the development of bone metastasis (1). PTHrP is produced by various types of carcinomas, including oral squamous cell carcinoma (OSCC) cells (2). HHM in patients with OSCC attributed to PTHrP appears to be an ominous prognostic sign (3). It has recently been reported that the coexpression of PTHrP and its type 1 receptor (PTHR1) in early breast cancer predicts poor patient survival (1). Furthermore, a mutant PTHR1 is a candidate gene for enchondroma, common benign cartilage tumors of the bone which have the potential for malignant transformation to chondrosarcoma (4).

PTHR1 is located on 3p22-p21.1. Chromosome 3p, which includes PTHR1 and thyroid hormone receptor ß (THRß) located on 3p24.1-p22, has one of the highest incidences of loss of heterozygosity (LOH) at loci for OSCC (5,6). LOH in the THRß gene has already been reported, and has been associated with reduced survival (7). However, the details of transformations including both LOH and microsatellite instability (MSI) in PTHR1 have not been extensively analyzed.

LOH and MSI are important events in the carcinogenesis of various types of carcinoma, including OSCC. LOH implies the loss of microsatellite loci, suggesting genetic loss, whereas MSI indicates replication error. Human carcinomas develop through a multistep process involving the activation of oncogenes and the inactivation of tumor suppressor genes (TSGs). Chromosomal regions with LOH indicate genomic regions which may harbor TSGs. Recently, the role of TSGs such as *p53*, *APC*, *BRCA1*, *BRCA2*, *DCC* and *FHIT* was analyzed in numerous human solid tumors (8-12).

The purpose of the present study was to elucidate the involvement of PTHR1 in the carcinogenesis of human sporadic OSCC.

Materials and methods

Patients and tumor samples. Seventeen OSCCs and their adjacent non-neoplastic tissues were obtained from surgical procedures performed at the Tohoku University Dental Hospital and the Sendai Medical Center, Japan. Diagnostic verification, tumor subtyping and grading were performed by pathologists. Grading and pathological criteria of oral carcinoma were determined using the TNM classification.

Correspondence to: Dr Hitoshi Miyashita, Division of Maxillofacial Surgery, Department of Oral Medicine and Surgery, Graduate School of Dentistry, Tohoku University, 4-1 Seiryo-mach, Aoba-ku, Sendai 980-8575, Japan
E-mail: miyashita@mail.tains.tohoku.ac.jp

Key words: loss of heterozygosity, microsatellite instability, endocrine hormone receptors, oral squamous cell carcinoma, carcinogenesis, thyroid hormone receptor ß, parathyroid hormone/parathyroid hormone-related protein type 1 receptor

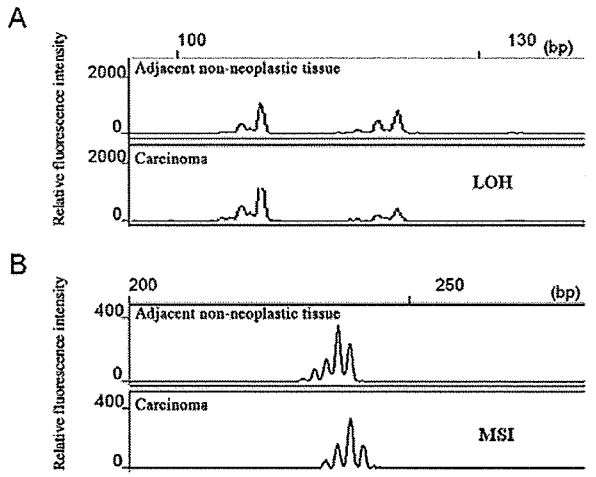

Figure 1. Representative result of (A) loss of heterozygosity (LOH) and (B) microsatellite instability (MSI) analysis in carcinoma tissue compared with adjacent non-neoplastic tissue.

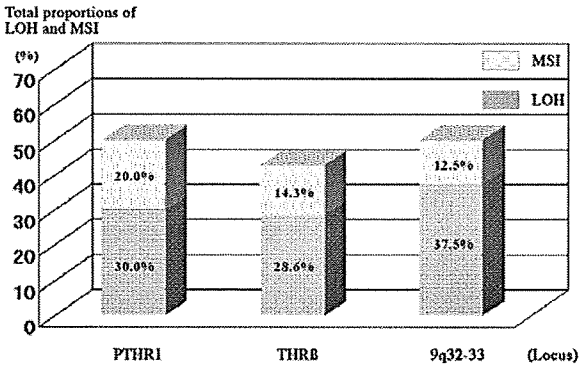

Figure 2. The proportions of loss of heterozygosity (LOH) and microsatellite instability (MSI) on loci including 3p21.2-14.2 (PTHR1), 3p24.1-21.3 (THRß) and 9q32-33.

The clinical and pathological characteristics of the cases are summarized in Table I.

DNA extraction. Before the tumor samples were processed for DNA extraction, sections from all the samples stained with hematoxylin and eosin underwent careful histopathological examination, which revealed the presence of a large amount of contaminating stroma. After deparaffinization of 10-μm sections stained with hematoxylin, neoplastic components were collected by a laser captured microdissection system (LMS, ver. 3.50, Carl Zeiss, Germany) to minimize the contamination of non-neoplastic stromal cells. Non-neoplastic tissues were used as normal controls. The dissected tissues were collected in an Eppendorf tube and incubated overnight at 58°C in digestion mixture (0.01 M NaCl, 0.5 M Tris-HCl, pH 8.0, 20 mM EDTA, 0.05% Tween-20R and 0.1 mg/ml proteinase K). The samples were then heated to 95°C for 10 min to inactivate proteinase K activity. After digestion, DNA was extracted with phenol/chloroform treatment and ethanol precipitation.

Analysis of LOH and MSI. The microsatellite markers used, all of which were purchased from Research Genetics (Huntsville, AL), are listed in Table I. Details regarding all markers can be found at the Genome Database (http://www.gdb.org). PCR reaction for LOH and MSI analysis was performed in a total volume of 10 μl containing 50 ng of DNA, dNTP at a final concentration of 20 μM, 0.4 μM of each primer and 0.25 U of Ex-Taq DNA polymerase (Takara Shuzo, Shiga, Japan). After the mixture was heated for 10 min at 94°C, PCR was performed for 45 cycles at 94°C at the appropriate annealing temperature and at 72°C for 1 min, each followed by 72°C for 10 min. After denaturation of the PCR products at 94°C for 2 min, samples were subjected to electrophoresis using a Performance Optimized Polymer 4 in a 310 Genetic Analyzer (Applied Biosystems, Foster, CA).

LOH analysis was performed at loci which included two endocrine hormone receptor genes and six tumor suppressor genes, and also at nine loci with frequencies of LOH reported in OSCC (Table I). All markers used were dye-labeled. LOH was defined as a reduction of ≥50% in the band intensity of one of the tumor sample alleles when compared by Gene Scan version 2.1 to a homozygous normal tissue control (Fig. 1A). Cases with a homozygous normal tissue pattern were not informative for LOH analysis. For MSI analysis, eight microsatellite markers recommended by the National Cancer Institute for the detection of MSI were used (Table I). A locus with shifted bands or extra bands as compared to normal controls was defined as MSI-positive (Fig. 1B).

Results

LOH at loci on chromosomes including endocrine hormone receptors. We examined LOH at two loci on chromosomes including PTHR1 and THRß. The results of LOH analysis are shown in Tables I and II. The proportions of allele losses on 3p22.-21.1 (candidate gene, PTHR1) and 3p24.1-22 (THRß) were 30.0% (3/10, LOH cases/informative cases) and 28.6% (2/7) in the human microdissected OSCC tissues, respectively. The frequencies of LOH in THRß were similar to those of previous studies. As a result, the proportion of cases with at least one LOH at these loci was 23.5% (4/17).

MSI in OSCC. Only two cases reached MSI at one locus of the TSGs, on 18q21 (DCC) and 3p21.1-14.2 (FHIT). However, the proportions of MSI on 8p21.1-11.2, 3p24.1-26.5 and 9p22 (IFNα) were 33.3 (3/10, MSI cases/ informative cases), 30.7 (4/13) and 27.3% (3/11), respectively. Furthermore, the proportions of MSI at loci on 3p22.-21.1 (PTHR1) and 3p24.1-22 (THRß) were 20.0 (2/10) and 14.3% (1/7), respectively. In contrast, the proportion of MSI with eight microsatellite markers was 0% (Tables I and II).

High frequency of LOH and MSI at loci in OSCC. Total proportions of LOH and MSI at loci on 3p21.2-14.2 (PTHR1), 3p24.1-21.3 (THRß) and 9q32-33 reached 50.0 (5/10, LOH and MSI cases/informative cases), 42.9 (3/7) and 50.0% (4/8), respectively (Fig. 2). Moreover, at loci on 3p24.1-26.5 and 8p21.1-11.2, proportions were 46.1 (6/13) and 40.0% (4/10), respectively.

LOH of the PTHR1-mediated carcinogenic pathway independent of TSGs. We examined LOH on chromosomes where novel

Table I. Loss of heterozygosity and microsatellite instabililty analysis in OSCC.

Sample no.			1	2	3	4	5	6	7	8	9	10	11	12	13	14	15	16	17
Stage			I	III	II	II	III	III	II	IV	IV	IV	III	I	II	II	II	IV	I
Histology			W	W	W	W	M	M	W	M	W	P	W	W	W	W	M	W	W
Gene	Position	Locus																	
Endocrine hormone receptor																			
PTHR1	3p21.1	D3S1606	▲	○	○	▲	–	○	–	–	○	●	–	●	●	△	○	△	△
THRß	3p24.1	THRß	△	△	●	△	○	–	–	▲	○	△	○	○	●	△	△	–	–
Tumor suppressor gene																			
p53	17q13.3	TP53	○	○	●	●	○	●	○	○	○	○	△	△	△	–	△	●	○
APC	5q21-22	D5S346	○	○	○	●	○	○	○	○	○	●	–	○	○	○	○	○	△
BRCA1	17q21	D17S579	○	○	–	○	○	○	○	○	○	○	–	–	–	–	–	–	●
BRCA2	13q12	D13S267	–	○	–	○	○	○	○	○	△	△	○	○	○	○	△	○	●
DCC	18q21	D18S59	–	○	○	○	●	○	○	○	○	▲	–	○	○	○	○	–	–
FHIT	3p21.1-14.2	D3S1300	○	○	○	○	○	–	○	○	○	○	–	○	▲	△	○	△	●
The frequency of LOH reported at loci for OSCC																			
	3p14.1-12	D3S1562	–	○	–	–	○	○	○	○	○	○	△	○	△	●	○	△	○
	3p14.1-13	D3S1296	○	○	○	–	○	○	●	○	–	○	△	○	△	–	△	△	–
	3p24.1-26.5	D3S192	○	○	▲	–	○	●	▲	○	–	●	○	○	▲	▲	○	–	–
	8p21.1-11.2	D8S298	▲	○	–	–	○	–	–	○	▲	●	△	○	△	▲	○	△	○
	9p21	D9S171	–	○	–	○	○	○	△	●	○	●	△	△	△	△	△	–	–
	9p22	IFNα	○	▲	○	▲	○	○	○	–	○	○	△	△	△	▲	○	–	△
	9p23-22	D9S162	○	–	○	○	–	○	△	●	○	●	△	○	△	△	△	○	●
	9p24	D9S286	○	●	–	–	●	○	○	○	–	○	△	○	△	△	○	–	○
	9q32-33	D9S177	–	△	–	○	–	△	△	●	○	●	○	○	–	▲	●	–	–
Microsatellite instability																			
	2p16	BAT25	○	○	○	○	○	○	○	○	○	○	△	○	△	○	○	○	○
	2p16	D2S123	○	○	○	○	○	○	○	○	○	●	○	○	○	○	○	○	○
	8p12	D8S87	○	○	○	○	○	○	○	○	–	–	○	○	○	–	△	○	–
	13q11	D13S175	○	○	○	○	○	○	○	○	–	○	○	○	△	○	○	–	●
	13q14.1-14.3	D13S153	○	○	○	●	○	○	○	○	–	○	○	–	△	○	○	–	○
	17q11.2-12	D17S250	○	○	○	○	○	○	○	○	○	○	△	○	○	○	○	○	○
	18q22.1	D18S55	○	○	○	○	○	○	○	○	○	○	△	○	○	○	○	○	–
	20p	D20S100	○	○	○	○	○	○	○	○	○	○	○	○	○	○	○	–	○

●, LOH; ○, normal; △, non-infomative; –, reaction failure; ▲, MSI. W, well-differentiated; M, moderately differentiated; P, poorly differentiated.

Table II. Proportion of loss of heterozygosity and microsatellite instability in OSCC.

Gene	Locus	MSI/inf (%)	LOH/inf (%)
Endocrine hormone receptor			
PTHR1	D3S1606	2/10 (20.0)	3/10 (33.3)
THRβ	THRß	1/7 (14.3)	2/7 (28.6)
Tumor suppressor gene			
p53	TP53	0/12 (0.0)	4/12 (33.3)
APC	D5S346	0/15 (0.0)	2/15 (13.3)
BRCA1	D17S579	0/10 (0.0)	1/10 (10.0)
BRCA2	D13S267	0/12 (0.0)	1/12 (8.3)
DCC	D18S59	1/13 (7.7)	1/13 (7.7)
FHIT	D3S1300	1/13 (7.7)	1/13 (7.7)
Frequency of LOH reported at loci for OSCC			
	D3S1562	0/11 (0.0)	1/11 (9.1)
	D3S1296	0/9 (0.0)	1/9 (11.1)
	D3S192	4/13 (30.7)	2/13 (15.4)
	D8S298	3/10 (30.0)	1/10 (10.0)
	D9S171	0/7 (0.0)	2/7 (28.6)
	IFNα	3/11 (27.3)	0/11 (0.0)
	D9S162	0/10 (0.0)	3/10 (30.0)
	D9S286	0/10 (0.0)	2/10 (20.0)
	D9S177	1/8 (12.5)	3/8 (37.5)
Microsatellite instability			
	BAT25	1/15 (6.7)	0/15 (0.0)
	D2S123	0/17 (0.0)	1/17 (5.9)
	D8S87	0/14 (0.0)	0/14 (0.0)
	D13S175	0/15 (0.0)	1/15 (6.7)
	D13S153	0/14 (0.0)	1/14 (7.1)
	D17S250	0/16 (0.0)	0/16 (0.0)
	D18S55	0/15 (0.0)	0/15 (0.0)
	D20S100	0/16 (0.0)	0/16 (0.0)

MSI/inf, number of microsatellite instability/informative cases; LOH/inf, number of loss of heterozygosity/informative cases.

TSGs such as *p53*, *APC*, *DCC*, *BRCA1*, *BRCA2* and *FHIT* were located, in order to evaluate the independence of LOH on the chromosome of PTHR1. As shown in Tables I and II, the proportions of LOH on 17q13.3 (candidate gene, p53), 5q21-22 (APC), 17q21 (BRCA1), 13q12 (BRCA2), 18q21 (DCC) and 3p21.2-14.2 (FHIT) were 33.3, 13.3, 10.0, 8.3, 7.7 and 7.7%, respectively. The proportion of carcinomas with LOH on the chromosome of PTHR1 but without LOH of novel TSGs was 20.0% (2/10).

Discussion

LOH analysis for PTHR1 was performed with the proportion of LOH on PTHR1 reaching 30.0% (3/10 cases) in human sporadic OSCC. In total, 4 of 15 cases (26.7%) revealed LOH in endocrine hormone receptors including PTHR1 and THRß. Although the proportion of PTHR1 was not high, it suggests that an anomaly of PTHR1 could be one of the crucial steps in carcinogenesis in human OSCC.

Microsatellites are widely-distributed repetitive DNA sequences composed of short tandemly-repeated nucleotide motifs. In some neoplasms, these sequences exhibit a form of genetic instability characterized by the gain or loss of repeat units at multiple independent loci. Such transformations have been observed to accumulate in cells defective for DNA repair activities. MSI has also been observed in a variety of sporadic malignancies (13-16), and plays an important role in the carcinogenesis of human carcinoma (13). Although the proportion of MSI with eight microsatellite markers was 0%, MSI on PTHR1 was revealed to be 20% (2/10 cases).

Our results suggest that the carcinogenesis of 30.0% of OSCCs might be due to abnormalities in PTHR1. Two cases revealed LOH in PTHR1, but no LOH was found in tumor suppressor genes (TSGs) such as *p53*, *FHIT*, *APC*, *BRCA1*, *BRCA2* and *DCC*. This indicates that LOH of the PTHR1-mediated carcinogenic pathway is independent of that of TSGs in human OSCC.

According to recent studies, coexpression of PTHrP and PTHR1 predicts poor patient survival in breast carcinoma (1). Coexpression of PTHrP and PTHR1 was also prevalent in paired primary prostate cancer and bone metastases (17). This coexpression suggests that autocrine PTHrP-mediated

stimulation may be a mechanism of escape from normal growth regulatory pathways. More importantly, positive PTHR1 expression in early breast cancer is linked with reduced patient survival (1). PTHR1 is also expressed in breast cancer bone metastasis and promotes autocrine proliferation in breast carcinoma cells (18). The presence of PTHR1 in the primary tumor, as opposed to PTHR1 itself, plays a dominant role in determining clinical outcome. The increased frequency and level of PTHR1 expression in bone metastases compared to primary tumors suggest that the receptor may play a role in the metastatic process. Therefore, as has been reported, treatment designed to inhibit PTHR1 function, such as monoclonal antibodies or synthetic antagonists (19,20), may offer improved clinical outcome in patients with carcinomas expressing PTHR1 (1).

In human OSCC, it has been reported that tumor-derived PTHrP may act locally to influence tumor growth as well as the differentiation and resorption of bone (21). Moreover, the clinical syndrome of humoral hypercalcemia of malignancy (HHM), attributed to PTHrP, has been implicated as an important factor in the development of bone metastasis and appears to be a prognostic sign (3). However, PTHR1 expression and its role in human OSCC has not yet been investigated and remains unclear. Our results indicate that, although no correlation was found between LOH in PTHR1 and clinical factors including tumor stage and histology, it is possibile that the transformation of PTHR1 may be involved in carcinogenesis in human OSCC.

Because LOH analysis is suggestive of TSG candidates, further evidence is required to verify that abnormality of PTHR1 contributes to carcinogenesis. We plan to further investigate the expression of PTHR1 or the coexpression of PTHrP and PTHR1 using immunohistochemical analysis, and to examine the relationship between their expression and clinical implications including tumor development, metastasis and patient survival in human sporadic OSCC.

References

1. Linforth R, Anderson N, Hoey R, Nolan T, Downey S, Brady G, Ashcroft L and Bundred N: Coexpression of parathyroid hormone related protein and its receptor in early breast cancer predicts poor patient survival. Clin Cancer Res 8: 3172-3177, 2002.
2. Tsuchimochi M, Kameta A, Sue M and Katagiri M: Immunohistochemical localization of parathyroid hormone-related protein (PTHrP) and serum PTHrP in normocalcemic patients with oral squamous cell carcinoma. Odontology 93: 61-71, 2005.
3. Iwase M, Kurachi Y, Kakuta S, Sakamaki H, Nakamura-Mitsuhashi M and Nagumo M: Hypercalcemia in patients with oral squamous cell carcinoma. Clin Oral Investig 5: 194-198, 2001.
4. Hopyan S, Gokgoz N, Poon R, Gensure RC, Yu C, Cole WG, Bell RS, Juppner H, Andrulis IL, Wunder JS and Alman BA: A mutant PTH/PTHrP type I receptor in enchondromatosis. Nat Genet 30: 306-310, 2002.
5. Roz L, Wu CL, Porter S, Scully C, Speight P, Read A, Sloan P and Thakker N: Allelic imbalance on chromosome 3p in oral dysplastic lesions: an early event in oral carcinogenesis. Cancer Res 56: 1228-1231, 1996.
6. Ishwad CS, Ferrell RE, Rossie KN, Appel BN, Johnson JT, Myers EN, Law JC, Srivastava S and Gollin SM: Loss of heterozygosity of the short arm of chromosomes 3 and 9 in oral cancer. Int J Cancer 69: 1-4, 1996.
7. Partridge M, Emilion G, Pateromichelakis S, A'Hern R, Lee G, Phillips E and Langdon J: The prognostic significance of allelic imbalance at key chromosomal loci in oral cancer. Br J Cancer 79: 1821-1827, 1999.
8. Werness BA, Parvatiyar P, Ramus SJ, Whittemore AS, Garlinghouse-Jones K, Oakley-Girvan I, DiCioccio RA, Wiest J, Tsukada Y, Ponder BA and Piver MS: Ovarian carcinoma in situ with germline BRCA1 mutation and loss of heterozygosity at BRCA1 and TP53. J Natl Cancer Inst 92: 1088-1091, 2000.
9. Levy DB, Smith KJ, Beazer-Barclay Y, Hamilton SR, Vogelstein B and Kinzler KW: Inactivation of both APC alleles in human and mouse tumors. Cancer Res 54: 5953-5958, 1994.
10. Horii A, Nakatsuru S, Ichii S, Nagase H and Nakamura Y: Multiple forms of the APC gene transcripts and their tissue-specific expression. Hum Mol Genet 2: 283-287, 1993.
11. Reale MA, Hu G, Zafar AI, Getzenberg RH, Levine SM and Fearon ER: Expression and alternative splicing of the deleted in colorectal cancer (DCC) gene in normal and malignant tissues. Cancer Res 54: 4493-4501, 1994.
12. Croce CM, Sozzi G and Huebner K: Role of FHIT in human cancer. J Clin Oncol 17: 1618-1624, 1999.
13. Parsons R, Li GM, Longley MJ, Fang WH, Papadopoulos N, Jen J, de la Chapelle A, Kinzler KW, Vogelstein B and Modrich P: Hypermutability and mismatch repair deficiency in RER$^+$ tumor cells. Cell 75: 1227-1236, 1993.
14. Gonzalez-Zulueta M, Ruppert JM, Tokino K, Tsai YC and Spruck CHd: Microsatellite instability in bladder cancer. Cancer Res 53: 5620-5623, 1993.
15. Thibodeau SN, Bren G and Schaid D: Microsatellite instability in cancer of the proximal colon. Science 260: 816-819, 1993.
16. Uchida T, Wada C, Wang C, Egawa S, Ohtani H and Koshiba K: Genomic instability of microsatellite repeats and mutations of H-, K-, and N-ras, and p53 genes in renal cell carcinoma. Cancer Res 54: 3682-3685, 1994.
17. Bryden AA, Hoyland JA, Freemont AJ, Clarke NW and George NJ: Parathyroid hormone related peptide and receptor expression in paired primary prostate cancer and bone metastases. Br J Cancer 86: 322-325, 2002.
18. Hoey RP, Sanderson C, Iddon J, Brady G, Bundred NJ and Anderson NG: The parathyroid hormone-related protein receptor is expressed in breast cancer bone metastases and promotes autocrine proliferation in breast carcinoma cells. Br J Cancer 88: 567-573, 2003.
19. Morley P, Whitfield JF and Willick GE: Design and applications of parathyroid hormone analogues. Curr Med Chem 6: 1095-1106, 1999.
20. Rabbani SA: Molecular mechanism of action of parathyroid hormone-related peptide in hypercalcemia of malignancy: Therapeutic strategies (Review). Int J Oncol 16: 197-206, 2000.
21. Dunne FP, Bowden SJ, Brown JS, Ratcliffe WA and Browne RM: Parathyroid hormone related protein in oral squamous cell carcinomas invading the mandible. J Clin Pathol 48: 300-303, 1995.

Pathology International 2008; **58**: 407–414 doi:10.1111/j.1440-1827.2008.02245.x

Original Article

Novel recombinant congenic mouse strain developing arthritis with enthesopathy

Shiro Mori,[1] Naoko Tanda,[1] Mitsuko R. Ito,[2] Hisashi Oishi,[2] Takahito Tsubaki,[2] Hiroaki Komori,[2] Ming-Cai Zhang,[3] Masao Ono,[3] Masahiko Nishimura[4] and Masato Nose[2]

[1]*Tohoku University Graduate School of Dentistry,* [3]*Tohoku University Graduate School of Medicine, Sendai,* [2]*Ehime University Graduate School of Medicine, Ehime and* [4]*Nagoya University Graduate School of Medicine, Nagoya, Japan*

Based on the hypothesis that the complex pathological and immunological manifestations of rheumatoid arthritis (RA) and the related diseases are under the control of multiple gene loci with allelic polymorphism, a recombinant congenic mouse strain was prepared between an MRL/Mp-*lpr/lpr* (MRL/lpr) strain, which develops arthritis resembling RA, and a non-arthritic strain C3H/HeJ-*lpr/lpr* (C3H/lpr). In MRL/lpr × (MRL/lpr × C3H/lpr) F1 mice, the mice developing severe arthritis were selected based on joint swelling to further continue intercrosses, and then an McH-*lpr/lpr*-RA1 (McH/lpr-RA1) strain was established and its histopathological phenotypes of joints and autoimmune traits were analyzed. Arthritis in McH/lpr-RA1 mice developed at a higher incidence by 20 weeks of age, compared with that in the MRL/lpr mice, who had severe synovitis (ankle, 60.3%; knee, 65.1%), and also fibrous and fibrocartilaginous lesions of articular ligamenta resembling enthesopathy (ankle, 79.4%; knee, 38.1%), resulting in ankylosis. The lymphoproliferative disorder was less, and serum levels of IgG and IgG autoantibodies including anti-dsDNA and rheumatoid factor were lower than those of both MRL/lpr and C3H/lpr strains. McH/lpr-RA1 mice may provide a new insight into the study of RA regarding the common genomic spectrum of seronegative RA and enthesopathy.

Key words: ankylosis, enthesitis, MRL/ lpr, rheumatoid arthritis, rheumatoid factor, seronegative, synovitis

Rheumatoid arthritis and the related diseases such as spondyloarthropathy and juvenile idiopathic arthritis show complex pathological manifestations of articular lesions, involving synovitis, enthesitis, and/or abnormal proliferation of bone and cartilage.[1,2] In general, disease categories with complex pathological manifestations have been defined based on clinical criteria, but pathology of the critical lesions in disease could reflect the specific phenotypes regarding pathogenesis. Recent studies of mouse genomics to dissect pathological phenotypes could provide a new insight into this subject,[3–8] leading to the hypothesis that complex pathological phenotypes of diseases are under the control of multiple gene loci with allelic polymorphism.

According to this hypothesis, we examined remodeling of articular lesions in an MRL strain of mice bearing a Fas antigen deletion mutant, MRL/MpJ-*lpr/lpr* (MRL/lpr)[9] with genome recombination. MRL/lpr mice spontaneously develop collagen diseases involving arthritis, which resembles rheumatoid arthritis (RA) in that they exhibit many of the serological characteristics of RA, including increased serum levels of antinuclear antibodies, circulating immune complexes, and IgM- and IgG- rheumatoid factors (RF).[10–12] Moreover, the histopathological features of the articular lesions in these mice are characterized by synovial cell proliferation, inflammatory cell infiltration, granulomatous inflammation in synovial sublining tissue and pannus formation.[11,13,14] But the incidence of arthritis in these mice is <30%, and the severity is limited according to microscopic observations, moreover, the incidence of arthritis is not associated with joint swelling.

In the present study we first prepared backcross generation mice using a non-arthritis strain of mice, C3H/HeJ-*lpr/lpr* (C3H/lpr), MRL/lpr × (MRL/lpr × C3H/lpr) F1. Among these N2 mice, we observed mice developing arthritis of the ankle joints with macroscopic swelling. We then began to intercross the N2 mice by means of selection based on swelling of the ankle joints. Finally, we established a novel recombinant strain of mice, designated McH-*lpr/lpr*-RA1, which developed arthritis at a high incidence and with enthesopathy.

Correspondence: Masato Nose, MD, PhD, Department of Pathology, Division of Pathogenomics, Ehime University Graduate School of Medicine, Shitsukawa, Toon, Ehime 791-0295, Japan. Email: masanose@m.ehime-u.ac.jp

Received 3 January 2008. Accepted for publication 3 March 2008.

MATERIALS AND METHODS

Mice

MRL/lpr, C3H/lpr and MRL/Mp-+/+(MRL/+) mice were purchased from Jackson Laboratory, Bar Harbor, Maine, USA. Using the former two strains, we prepared backcross generation mice, MRL/lpr × (MRL/lpr × C3H/lpr) F1. Among the N2 mice, we observed the mice that developed arthritis, macroscopically manifested by ankle joint swelling. We then established a recombinant congenic strain of mice that developed arthritis by means of selection based on the swelling of ankle joints. From the generation F54, this recombinant congenic strain of mice was designated McH-*lpr/lpr*-RA1 (McH/lpr-RA1). These mice were housed in the Animal Research Institute of Tohoku University Graduate School of Medicine under specific pathogen-free and climate-controlled conditions with 12 h light–dark cycles, and each female and male littermate at 5 weeks of age was removed to cages (fewer than six per cage) separated from their parents to avoid fighting as much as possible.

Histopathology

At the indicated weeks of age, each mouse was bled under ether anesthesia. Sections of kidneys, heart, lungs, spleen, pancreas, salivary glands and lymph nodes were then fixed in 10% formalin in 0.01 mol/L phosphate buffer (pH 7.2) and embedded in paraffin. They were stained with HE, elastica-Masson (EM) and PAS for histological examination on light microscopy.

For ankle joints, serial sections were taken sagittally through the talus. The lesions, including calcaneus bone and anterior and posterior synovial tissue were histopathologically evaluated with the following grading system: normal, grade 0; thickening and proliferation of synovial lining, grade 1; grade 1 with granulomatous and/or fibrous lesions in synovial sublining tissue, grade 2; and grade 2 with pannus formation against bone cortex and/or bone marrow, grade 3. For knee joints, serial sections were prepared sagittally through the patella. The articular lesions including the tibia, femur, meniscus, plica alaris and capsula articularis were similarly evaluated as described in the previous section. We categorized grade 0 or 1 individuals as synovitis negative, and grade 2 or 3 individuals as synovitis positive.

The presence of ankylosis of the ankle and knee joints was also evaluated as follows: normal, grade 0; fibrous and fibrocartilage proliferative lesions in joints involving articular ligamenta and periostea, slight, grade 1; lesions similar to grade 1, moderate, grade 2; and lesions similar to grade 2, associated with bone destruction, grade 3. We categorized individuals with a score of higher than grade 1 as ankylosis positive. The incidence of vasculitis or glomerulonephritis was calculated as described previously.[15]

Flow cytometry

Lymphoid cells from the lymph nodes and spleen were examined for surface markers on flow cytometry. The cells were treated with fluorescein isothiocyanate (FITC)-conjugated rat monoclonal antibodies to Thy1.2 (clone 3D-H12; Becton Dickinson, Bedford, CA, USA), and phycoerythrin (PE)-conjugated rat monoclonal antibodies to B220 (clone RA3.6B2; PharMingen, San Diego, CA, USA), with FITC-conjugated rat monoclonal antibodies to CD4 (clone GK1.5) and PE-conjugated rat monoclonal antibodies to CD8 (clone 53–6.7; PharMingen), or with FITC-conjugated goat polyclonal antibodies to IgG or IgM (Zymed, San Francisco, CA, USA). The Fas-expressing cells were analyzed using FITC-conjugated hamster monoclonal antibodies to Fas (clone Jo2; PharMingen). These cells were analyzed on FACSCalibur using the CellQuest program (Becton Dickinson, Franklin Lakes, NJ, USA).

Immunoglobulin and autoantibody serum level

The serum levels of immunoglobulins involving IgG and IgM were quantified on single radial immunodiffusion, using goat polyclonal antimouse IgG and IgM antibodies (Zymed), respectively. The amounts of each in the serum samples were estimated from a standard curve using mouse Ig standards (Bethyl Laboratories, Montgomery, TX, USA).

The relative amounts in the serum of double-stranded DNA (dsDNA) antibodies were determined on ELISA using calf thymus DNA (type I, Sigma Chemical, St. Louis, MO, USA) and alkaline phosphatase-conjugated rabbit polyclonal antibodies to mouse IgG (AP-antimouse IgG; Sigma) according to a method previously described.[16] Rheumatoid factor was measured as IgG antibodies that specifically bound to the recombinant Fc fragments derived from human IgG1.[17]

Statistical analysis

The association of each strain with the incidence of synovitis or ankylosis was evaluated using Fisher's exact test. The difference between each strain in the weight of spleen, axillary lymph nodes, and serum levels of IgG, IgM and autoantibodies was evaluated on Student's *t*-test. $P < 0.01$ was considered to be significant.

RESULTS

Higher incidence of arthritis and enthesopathy

Ankle joint swelling of McH/lpr-RA1 mice was significantly observed at later than 16 weeks of age (Fig. 1). At 20 weeks

of age, these mice microscopically showed severe inflammatory synovitis with pannus formation resembling that in MRL/lpr mice (Fig. 2a), but the incidence of synovitis in the ankle joints was remarkably higher (60.3%) than in the MRL/lpr mice (8.0%; Table 1). Similar lesions were frequently observed in the knee joints (Fig. 2b). The incidence of synovitis of knee joints in McH/lpr-RA1 mice was not significantly higher than that in the MRL/lpr mice (Table 1).

Among McH/lpr-RA1 mice, many individuals developed ankylosis in their ankle and knee joints. Ankylosis in this strain of mice was characterized by fibrous and fibrocartilage proliferative lesions in the joints involving articular ligamenta and periostea, partly occupying the joint space, resembling enthesopathy (Fig. 2c–f). These lesions seemed to be specific for McH/lpr-RA1 mice because no MRL/lpr and C3H/lpr mice developed these lesions (Table 2). Sex difference in ankylosis of McH/lpr-RA1 mice was not a significant factor in the ankle or knee joints ($P = 0.073$ and $P = 0.093$, respectively), thus indicating that ankylosis in these mice might not result from an aggressive behavior as is generally considered in male mice. It seemed that synovitis, at least in ankle joints, developed prior to ankylosis at 8 week of age because ankylosis in ankle joints was never observed in any McH/lpr-RA1 mice at 8 weeks of age (Tables 1,2). But the correlation between the synovitis grades and ankylosis grades, at least in the ankle joints at 20 weeks of age, was not significant (female, correlation coefficient: $r = -0.167$; male; $r = 0.404$; total, $r = 0.183$).

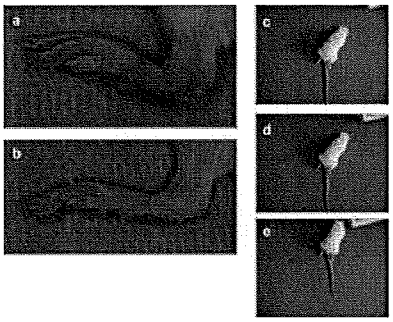

Figure 1 Joint swelling in McH/lpr-RA1 mice. A male McH/lpr-RA1 mouse at 16 week of age shows (**a**) significant swelling of ankle joint, compared with (**b**) an age-matched male MRL/lpr mouse. (**c–e**) Pictures clipped from the video film showing crippled walking of a male McH/lpr-RA1 mouse at 20 weeks of age due to ankylosis.

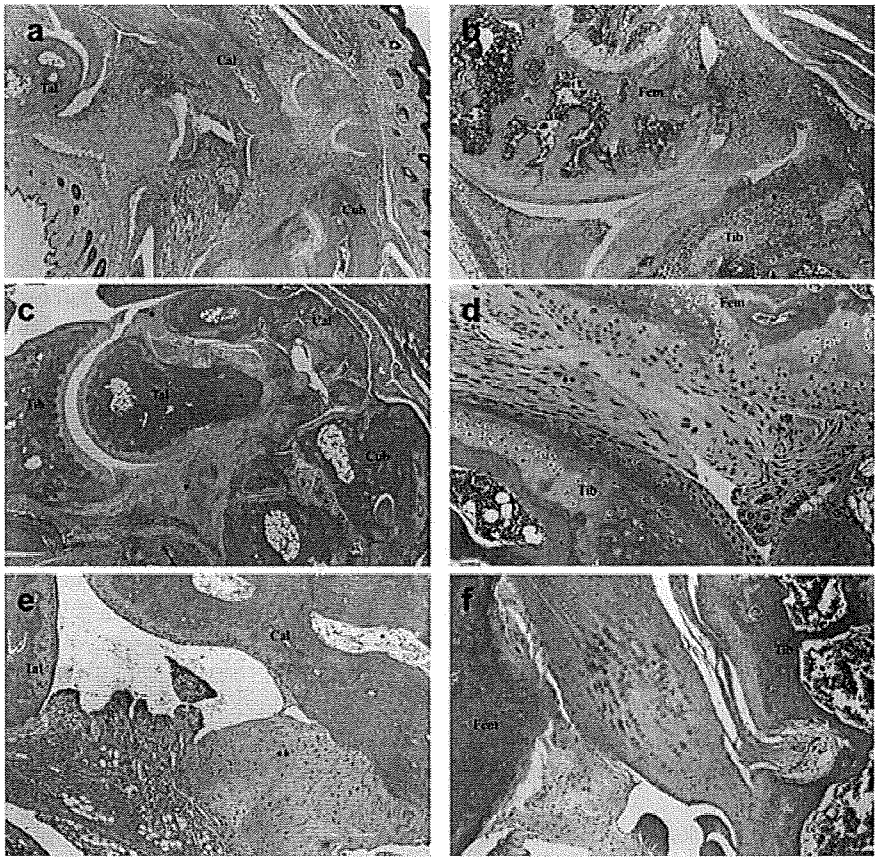

Figure 2 Representative histopathological features of articular lesions in McH/lpr–RA1 mice. (**a,c,e**) Ankle joints and (**b,d,f**) knee joints (HE). Cal, calcaneus; Cub, cuboidal bone; Fem, femur; Tal, talus; Tib, tibia. (**a**) Male mouse at 20 weeks of age shows severe inflammatory proliferative lesions of synovial tissues with pannus formation, evident against talus, calcaneus and cubic bones (synovitis grade 3). (**b**) Male mouse at 20 weeks of age developed synovitis corresponding to synovitis grade 3 showing severe pannus formation (*), invading into tibia bone. (**c**) Ankylosis in a male mouse at 20 weeks of age, characteristic of the proliferative lesions of fibrocartilage, but not hyaline cartilage, especially marked in articular ligament around talus bone (*; ankylosis grade 3). (**d**) Ankylosis of a male mouse at 8 weeks of age showing fibrocartilaginous change of the intra-articular ligament (**; ankylosis grade 1) associated with grade 1 synovitis (*). (**e**) Synovitis with inflammatory fibrosis in the sublining region (*; grade 2) and ankylosis with destruction of calaneus (**; grade 3) in a male mouse at 20 weeks of age. (**f**) Fibrocartilaginous change of intra-articular ligament, associated with the growth of chondrocytes (ankylosis), and synovitis with pannus (*), characteristically with the presence of osteoclasts, in a male mouse at 20 weeks of age.

Table 1 Incidence of synovitis in McH/lpr-RA1, MRL/lpr and C3H/lpr mice

	Grade of synovitis					
	0	1	2	3	Incidence of positive mice, *n* (%)†	
Ankle joints						
McH/lpr-RA1 (20 week old)						
Female	0	8	0	12	12/20	(60.0)
Male	0	17	1	25	26/43	(60.5)
Total	0	25	1	37	38/63	(60.3)‡
McH/lpr-RA1 (8 week old)						
Female	0	17	0	0	0/17	(0.0)
Male	0	15	1	1	2/17	(11.8)
Total	0	32	1	1	2/34	(5.9)
MRL/lpr (20 week old)						
Female	8	2	0	1	1/11	(9.1)
Male	9	4	1	0	1/14	(7.1)
Total	17	6	1	1	2/25	(8.0)
C3H/lpr (20 week old)						
Female	17	8	0	0	0/25	(0.0)
Male	20	1	0	2	2/23	(0.1)
Total	37	9	0	2	2/48	(4.2)
Knee joints						
McH/lpr-RA1 (20 week old)						
Female	0	2	0	18	18/20	(90.0)§
Male	1	19	1	22	23/43	(53.5)
Total	1	21	1	40	41/63	(65.1)#
McH/lpr-RA1 (8 week old)						
Female	0	5	0	12	12/17	(70.6)
Male	0	7	0	10	10/17	(58.8)
Total	0	12	0	22	22/34	(64.7)
MRL/lpr (20 week old)						
Female	6	0	0	5	5/11	(45.5)
Male	5	3	0	6	6/14	(42.9)
Total	11	3	0	11	11/25	(44.0)
C3H/lpr (20 week old)						
Female	25	0	0	0	0/25	(0.0)
Male	22	1	0	0	0/23	(0.0)
Total	47	1	0	0	0/48	(0.0)

‡$P = 0.0014$ vs MRL/lpr mice, Fisher's exact test; §$P = 0.215$ vs female MRL/lpr mice, Fisher's exact test; #$P = 0.228$ vs MRL/lpr mice, Fisher's exact test.

†No. synovitis-positive mice (grades 2 and 3)/total number examined (%).

Development of vasculitis, but no glomerulonephritis

McH/lpr-RA1 mice coincidentally developed vasculitis, but not glomerulonephritis. The incidence of vasculitis in kidney was similar to that in MRL/lpr mice at 20 weeks of age (McH/lpr-RA1, 63/63; MRL/lpr, 17/25; $P = 0.186$). The histopathological features of vasculitis were characteristic of granulomatous arteritis, similar to those of MRL/lpr mice (data not shown). In contrast, the incidence of glomerulonephritis was significantly different (McH/lpr-RA1, 12/63; MRL/lpr, 17/25; $P < 0.004$). This may be the reason why the McH/lpr-RA1 mice lived remarkably longer than the MRL/lpr mice.

Dissociation from lymphoproliferative disorder

Importantly, all mice of the McH/lpr-RA1 strain had only mild splenomegaly and lymphadenopathy (spleen, 0.275 ± 0.145 g; lymph nodes, 0.174 ± 0.164 g), different from the original strains of MRL/lpr (spleen, 0.531 ± 0.199 g, $P < 0.001$; lymph nodes, 0.730 ± 0.298 g, $P < 0.001$) and C3H/lpr mice (spleen, 0.562 ± 0.189 g, $P < 0.001$; lymph nodes, 0.875 ± 0.288 g, $P < 0.001$), although there was no difference between MRL/lpr and C3H/lpr mice in spleen and lymph nodes ($P > 0.01$).

The accumulation of $Thy1^+B220^+$ T cells into the spleen and lymph nodes, which is a characteristic phenotype of the *lpr* gene,[18] was not remarkable, in comparison to that in MRL/lpr and C3H/lpr mice (Fig. 3a). This seemed to reflect the decrease of the double negative ($CD4^-CD8^-$) T cells in the spleen and lymph nodes and, in contrast, the increase of $CD4^+$ T cells and especially $CD8^+$ T cells (Fig. 3b). As a result, the CD4/CD8 ratio of spleen cells and lymph node cells was found to be remarkably lower in the McH/lpr-RA1 mice than in the MRL/lpr or C3H/lpr mice, although the high CD4/CD8 ratio in *lpr*-bearing mice is thought to result from the absence of Fas-mediated apoptosis in $CD4^+$ T cells.[15] But the expres-

Table 2 Incidence of ankylosis in McH/lpr-RA1, MRL/lpr and C3H/lpr mice

	Grade of ankylosis					
	0	1	2	3	Incidence of positive mice, *n* (%)†	
Ankle joints						
McH/lpr-RA1 (20 weeks old)						
Female	11	6	3	0	9/20	(45.0)
Male	2	9	14	18	41/43	(95.3)
Total	13	15	17	18	50/63	(79.4)**
McH/lpr-RA1 (8 weeks old)						
Female	17	0	0	0	0/17	(0.0)
Male	17	0	0	0	0/17	(0.0)
Total	34	0	0	0	0/34	(0.0)
MRL/lpr (20 weeks old)						
Female	11	0	0	0	0/11	(0.0)
Male	14	0	0	0	0/14	(0.0)
Total	25	0	0	0	0/25	(0.0)
C3H/lpr (20 weeks old)						
Female	25	0	0	0	0/25	(0.0)
Male	23	0	0	0	0/23	(0.0)
Total	48	0	0	0	0/48	(0.0)
Knee joints						
McH/lpr-RA1 (20 weeks old)						
Female	8	10	2	0	12/20	(60.0)
Male	31	11	1	0	12/43	(27.9)
Total	39	21	3	0	24/63	(38.1)***
McH/lpr-RA1 (8 weeks old)						
Female	16	1	0	0	1/17	(5.9)
Male	16	1	0	0	1/17	(5.9)
Total	32	2	0	0	2/34	(5.9)
MRL/lpr (20 weeks old)						
Female	11	0	0	0	0/11	(0.0)
Male	14	0	0	0	0/14	(0.0)
Total	25	0	0	0	0/25	(0.0)
C3H/lpr (20 weeks old)						
Female	25	0	0	0	0/25	(0.0)
Male	23	0	0	0	0/23	(0.0)
Total	48	0	0	0	0/48	(0.0)

**$P = 0.001$ vs MRL/lpr mice, Fisher's exact test; ***$P < 0.0001$ vs MRL/lpr mice, Fisher's exact test.
†No. positive mice (grades 1, 2 and 3)/total number examined (%).

sion of Fas in splenic cells and lymph node cells was remarkably lower than that in MRL/+mice: almost at the same level as that in MRL/lpr and C3H/lpr mice (Fig. 3c).

Dissociation from autoimmune traits

The serum levels of IgG in McH/lpr-RA1 mice were significantly lower than those of MRL/lpr and C3H/lpr mice, whereas the IgM level was similar to that in MRL/lpr mice (Fig. 4) although the number of IgG or IgM positive cells in the spleen and lymph node in this strain were relatively higher than those of MRL/lpr and C3H/lpr mice (Fig. 3d,e).

The serum levels of both IgG anti-dsDNA antibodies and IgG rheumatoid factors in McH/lpr-RA1 mice were remarkably low in comparison to those of both MRL/lpr and C3H/lpr mice (Fig. 5). These titers were almost the same in the McH/lpr-RA1 mice at 8 weeks of age (data not shown).

DISCUSSION

In the present study we established a novel recombinant congenic strain of mice, McH/lpr-RA1, which was started from the MRL/lpr × (MRL/lpr × C3H/lpr) F1 generation, by means of selection based on swelling in the ankle joints. In this strain, synovitis developed in the ankle joints at a higher incidence than that in the MRL/lpr mice, and ankylosis manifested by enthesopathy developed in the ankle and knee joints. This supports the idea that arthritis is controlled by polygenic inheritance. Namely, a particular genome combination with C3H/lpr alleles accelerates the incidence of synovitis and produces enthesopathy.

Such a genome recombination was also useful for evaluating several serological parameters that might be responsible for the development of diseases. McH/lpr-RA1 mice had a lower level of both IgM and IgG despite the presence of the *lpr* gene (Fig. 4a,b), and their IgG autoantibodies were fewer than in MRL/lpr and C3H/lpr mice (Fig. 5a,c). In previous

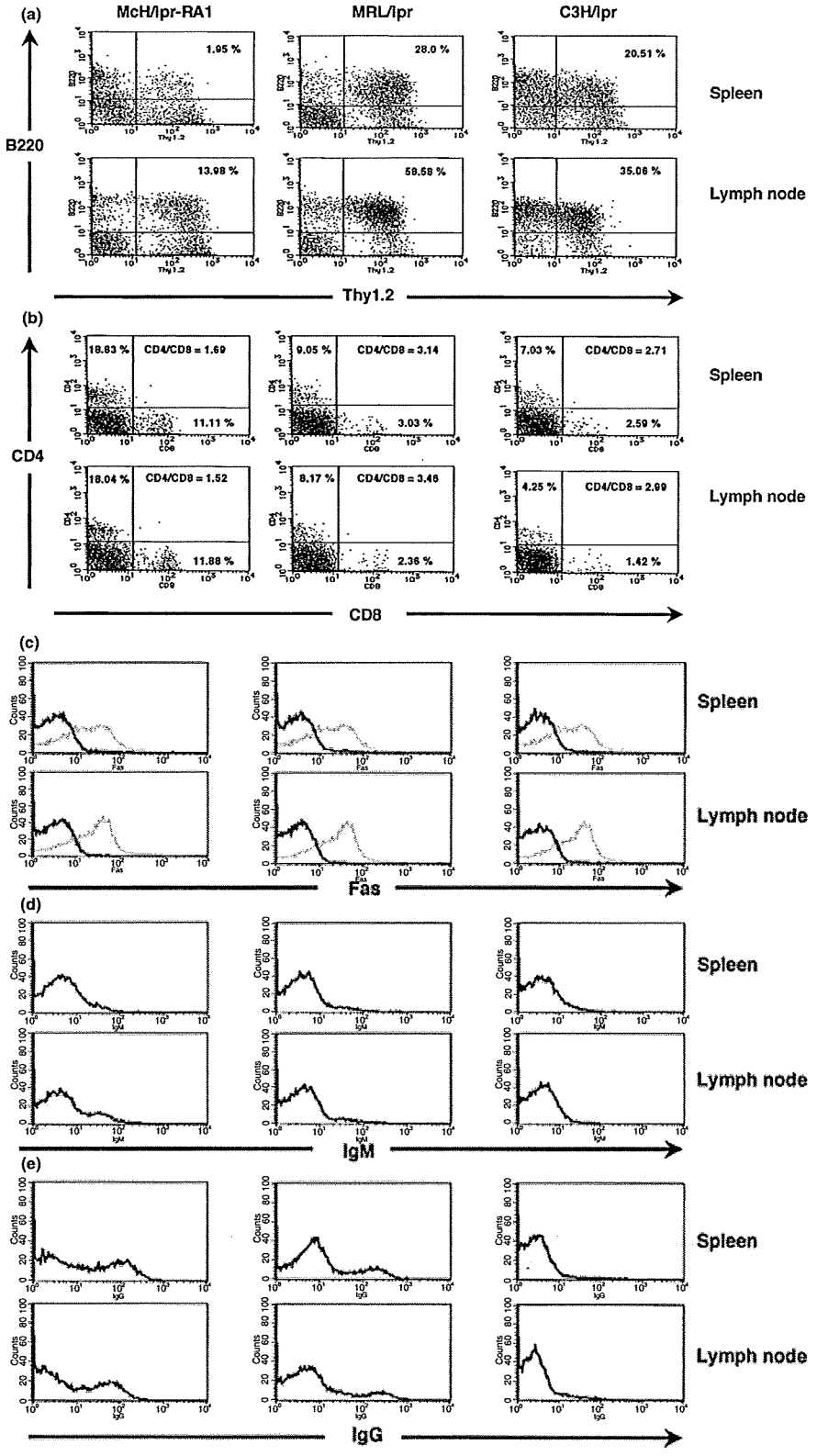

Figure 3 Flow cytometry of lymphocytes from spleen and lymph nodes from 20-week-old McH/lpr-RA1, MRL/lpr and C3H/lpr mice. Representative profiles of the cells were analyzed based on the expression of (**a**) Thy1.2 and B220, (**b**) CD4 and CD8, (**c**) Fas, (**d**) IgM and (**e**) IgG. For Fas antigen expression, 20-week-old MRL/+mice were used as controls (fine lines in c).

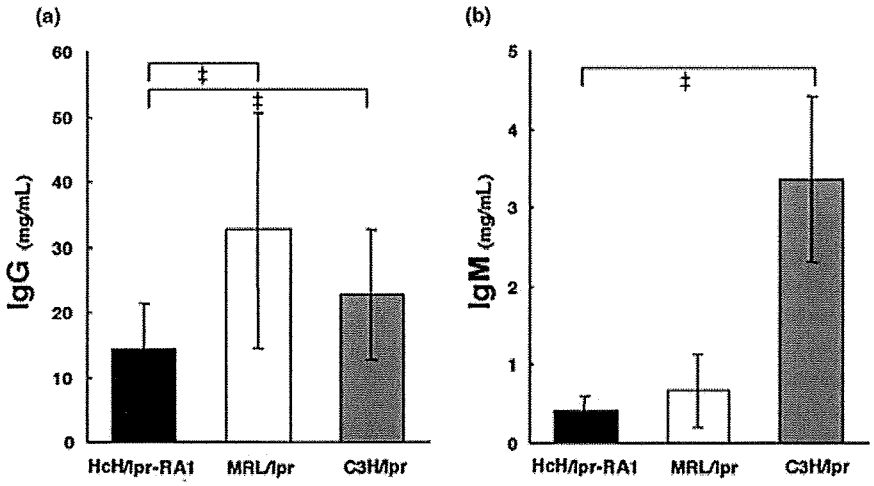

Figure 4 The serum levels of (a) IgG and (b) IgM. McH/lpr-RA1 ($n = 22$), MRL/lpr ($n = 20$) and C3H/lpr ($n = 20$) mice at 20 weeks of age (mean and SEM). ‡$P < 0.005$.

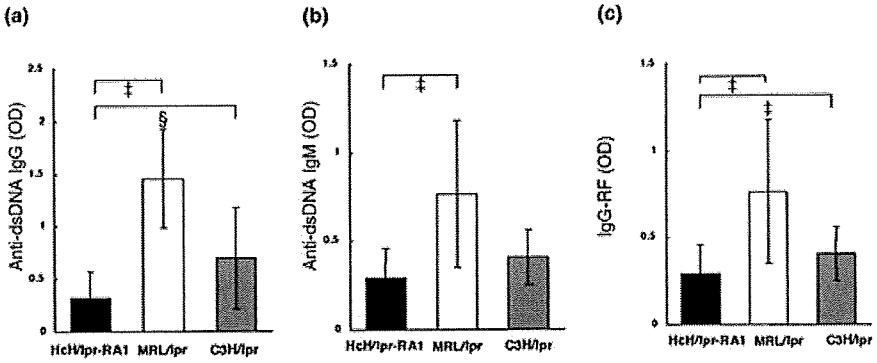

Figure 5 Serum levels of (a) IgG and (b) IgM anti-dsDNA antibodies and (c) IgG rheumatoid factors (RF). McH/lpr-RA1 ($n = 22$), MRL/lpr ($n = 20$) and C3H/lpr ($n = 20$) mice at 20 weeks of age (mean and SEM). OD, optical density. ‡$P < 0.005$; §$P < 0.01$.

studies in MRL/lpr mice, high serum levels of IgG rheumatoid factor seemed to play a critical role in the development of arthritis.[11,19] But it became clear in the present study that high serum levels of IgG rheumatoid factor as found in MRL/lpr mice are not necessary for the development of arthritis in McH/lpr-RA1 mice. As a result, the pathogenetic role of IgG rheumatoid factor on arthritis in MRL/lpr mice therefore needs to be re-evaluated.

Moreover, lymphoproliferative disorders manifested by splenomegaly and lymphadenopathy decreased in McH/lpr-RA1 mice in comparison to those in MRL/lpr and C3H/lpr mice, although the Fas deletion levels on the cell surface were almost the same among these three *lpr* strains (Fig. 3c). Throughout the repeated intercrossing for the establishment of the recombinant congenic strain, we observed that the lymph node weights seemed to decrease for each generation. Correspondingly, the accumulation of $Thy1^+B220^+$ T cells into spleen and lymph nodes decreased (Fig. 3a) while the ratio of CD4/CD8 decreased (Fig. 3b). This indicates that T-cell subsets in the periphery might be controlled by an allelic combination in the *lpr* mice, and that a mechanism besides Fas-mediated apoptosis has become accelerated in this strain. The expression levels of tumor necrosis factor-α should be further studied as one of the candidates inducing apoptosis,[20] which might also correlate with the higher incidence of synovitis in this strain.

It is important to elucidate whether ankylosis in the McH/lpr-RA1 mice might be the result of synovitis. In general, synovitis associated with pannus formation is though to lead ankylosis in RA, mainly characterized by the replacement of the joint surface by fibrous tissue derived from the invading pannus. Ankylosis in this strain of mice, however, seems to be due to enthesopathy, which was histopathologically manifested by the fibrous and fibrocartilaginous proliferation of enthesis, the site of insertion of a tendon, ligamenta or articular capsule into bone, similar to that previously described.[21] If that is the case, then synovitis in this strain of mice might be a result of secondary synovitis following enthesopathy.[22] But this is unlikely considering that the correlation between the synovitis grades and the ankylosis grades in the ankle joints of McH/lpr-RA mice at 20 weeks of age was not significant, and also that MRL/lpr mice developed synovitis in knee joints as often as McH/lpr-RA1 mice, but never developed ankylosis (Tables 1,2). As a result, the development of enthesopathy may be genetically independent from synovitis. Similar lesions to enthesopathy in McH/lpr-RA1 mice can be observed in male

DBA/1 mice that spontaneously develop the lesions in their ankles or lower extremities at older than 4 months of age, but these mice are not associated with severe synovitis.[23,24] We recently found that the severity and early onset of enthesopathy in DBA/1 mice were accelerated by a gene locus in an MRL allele, which was localized on chromosome 10 and designated Adm1.[25] This locus in McH/lpr-RA1 mice was an MRL homozygote, which involves several candidate genes mediating cellular proliferation and differentiation such as β2 integrin, basigin and macrophage migration inhibitory factor (MIF). In humans, *MIF* and *ITGB2* (β2 integrin) are associated with juvenile idiopathic arthritis.[26,27]

The present findings thus suggest that a diversity of pathological manifestations of arthritic lesions might be involved in a common genomic spectrum of collagen disease including RA, spondylarthropathy and juvenile idiopathic arthritis, especially enthesitis-related arthritis.[2]

ACKNOWLEDGMENTS

The authors are indebted to Ms S. Terasaki for technical help in animal care, and Ms E. Kondo and M. Terada for assistance with histopathology. This study was supported by Grant-in Aid for the Scientific Research Funds of the Ministry of Education, Science and Culture of Japan (S.M. 15390607, M.N. 18390123).

REFERENCES

1 Maini RN, Zvaifler NJ. Rheumatoid arthritis and spondyloarthropathy. In: Klippel JH, Dieppe PA, eds. *Rheumatology*. London: Mosby, 1994; 3.1.1–3.40.2.
2 Petty RE, Southwood TR, Baum J *et al.* Revision of the proposed classification criteria for juvenile idiopathic arthritis: Durban, 1997. *J Rheumatol* 1998; **25**: 1991–4.
3 Nose M, Nishimura M, Kyogoku M. Analysis of granulomatous arteritis in MRL/Mp autoimmune disease mice bearing lymphoproliferative genes. The use of mouse genetics to dissociate the development of arteritis and glomerulonephritis. *Am J Pathol* 1989; **135**: 271–80.
4 Nose M, Nishimura M, Ito MR, Itoh J, Shibata T, Sugisaki T. Arteritis in a novel congenic strain of mice derived from MRL/lpr lupus mice. *Am J Pathol* 1996; **149**: 1763–9.
5 Nishimura H, Nose M, Hiai H, Minato N, Honjo T. Development of lupus-like autoimmune diseases by disruption of the PD-1 gene encoding an ITIM motif-carrying immunoreceptor. *Immunity* 1999; **11**: 141–51.
6 Nose M, Nishihara M, Fujii H. Genetic basis of the complex pathological manifestations of collagen disease: Lessons from MRL/lpr and related mouse models. *Int Rev Immunol* 2000; **19**: 473–98.
7 Nishimura H, Okazaki T, Tanaka Y *et al.* Autoimmune dilated cardiomyopathy in PD-1 receptor-deficient mice. *Science* 2001; **291**: 319–22.
8 Kamogawa J, Terada M, Mizuki S *et al.* Arthritis in MRL/lpr mice is under the control of multiple gene loci with an allelic combination derived from the original inbred strains. *Arthritis Rheum* 2002; **46**: 1067–74.
9 Murphy ED, Roths JB. Autoimmunity and lymphoproliferation: Induction by mutant gene *lpr*, and acceleration by a male-associated factor in strain BXSB mice. In: Rose NR, Bigazzi PE, Warner NL, eds. *Genetic Control of Autoimmune Disease*. New York: Elsevier North Holland, 1978; 207–20.
10 Izui S, Eisenberg RA. Circulating anti-DNA-rheumatoid factor complexes in MRL/1 mice. *Clin Immunol Immunopathol* 1980; **15**: 536–51.
11 Hang L, Theofilopoulos AN, Dixon FJ. A spontaneous rheumatoid arthritis-like disease in MRL/1 mice. *J Exp Med* 1982; **155**: 1690–701.
12 Nardella FA, Teller DC, Izui S, Mannik M. Self-associating IgG rheumatoid factors in MRL/1 autoimmune mice. *Arthritis Rheum* 1982; **27**: 1165–73.
13 O'Sullivan FX, Fassbender HG, Gay S, Koopman WJ. Etiopathogenesis of the rheumatoid arthritis-like disease in MRL/1 mice. I. The histomorphologic basis of joint destruction. *Arthritis Rheum* 1985; **28**: 529–56.
14 Tarkowski A, Jonsson R, Holmdahl R, Klareskog L. Immunohistochemical characterization of synovial cells in arthritic MRL-*lpr/lpr* mice. *Arthritis Rheum* 1987; **30**: 75–82.
15 Wang Y, Nose M, Kamoto T, Nishimura M, Hiai H. Host modifier genes affect mouse autoimmunity induced by the *lpr* gene. *Am J Pathol* 1997; **151**: 1791–8.
16 Takahashi S, Nose M, Sasaki J, Yamamoto T, Kyogoku M. IgG3 production in MRL/lpr mice is responsible for development of lupus nephritis. *J Immunol* 1991; **147**: 515–20.
17 Nose M, Takano R, Nakamura S, Arata Y, Kyogoku M. Recombinant Fc of human IgG1 prepared in an *Escherichia coli* system escapes recognition by macrophages. *Int Immunol* 1990; **2**: 1109–12.
18 Morse HC III, Davidson WF, Yetter RA, Murphy ED, Roths JB, Coffman RL. Abnormalities induced by the mutant gene lpr: Expansion of unique lymphocyte subset. *J Immunol* 1982; **129**: 2612–15.
19 Otto JM, Cs-Szabo G, Gallagher J *et al.* Identification of multiple loci linked to inflammation and autoantibody production by a genome scan of a murine model of rheumatoid arthritis. *Arthritis Rheum* 1999; **42**: 2524–31.
20 Zheng L, Fisher G, Miller RE, Peschon J, Lynch DH, Lenardo MJ. Induction of apoptosis in mature T cells by tumour necrosis factor. *Nature* 1995; **377**: 348–51.
21 Niepel GA, Sitaj S. Enthesopathy. *Clin Rheum Dis* 1979; **5**: 857–87.
22 McGonagle D, Gibbon W, Emery P. Classification of inflammatory arthritis by enthesitis. *Lancet* 1998; **352**: 1137–40.
23 Holmdahl R, Jansson L, Andersson M, Jonsson R. Genetic, hormonal and behavioural influence on spontaneously developing arthritis in normal mice. *Clin Exp Immunol* 1992; **88**: 467–72.
24 Nordling C, Karlsson Parra A, Jansson L, Holmdahl R, Klareskog L. Characterization of a spontaneously occurring arthritis in male DBA/1 mice. *Arthritis Rheum* 1992; **35**: 717–22.
25 Oishi H, Miyazaki T, Mizuki S *et al.* Accelerating effect of an MRL gene locus on the severity and onset of arthropathy in DBA/1 mice. *Arthritis Rheum* 2005; **52**: 959–66.
26 Donn R, Alourfi Z, De Benedetti F *et al.* Mutation screening of the macrophage migration inhibitory factor gene: Positive association of a functional polymorphism of macrophage migration inhibitory factor with juvenile idiopathic arthritis. *Arthritis Rheum* 2002; **46**: 2402–9.
27 Fujita K, Kobayashi K, Okino F. Juvenile rheumatoid arthritis in two siblings with congenital leukocyte adhesion deficiency. *Eur J Pediatr* 1988; **148**: 118–19.

Research Article

Antitumor Effect of SN-38–Releasing Polymeric Micelles, NK012, on Spontaneous Peritoneal Metastases from Orthotopic Gastric Cancer in Mice Compared with Irinotecan

Takako Eguchi Nakajima,[1,2] Kazuyoshi Yanagihara,[3] Misato Takigahira,[3] Masahiro Yasunaga,[1] Ken Kato,[2] Tetsuya Hamaguchi,[2] Yasuhide Yamada,[2] Yasuhiro Shimada,[2] Keichiro Mihara,[5] Takahiro Ochiya,[4] and Yasuhiro Matsumura[1]

[1]Investigative Treatment Division, Research Center for Innovative Oncology, National Cancer Center Hospital East, Kashiwa, Chiba, Japan; [2]Gastrointestinal Oncology Division, National Cancer Center Hospital, [3]Central Animal Laboratory, and [4]Section for Studies on Metastasis, National Cancer Center Research Institute, Tokyo, Japan; and [5]Hematology and Oncology Department, Clinical and Experimental Oncology Division, Research Institute for Radiation Biology and Medicine, Hiroshima University, Hiroshima, Japan

Abstract

7-Ethyl-10-hydroxy-camptothecin (SN-38), an active metabolite of irinotecan hydrochloride (CPT-11), has potent antitumor activity. Moreover, we have reported the strong antitumor activity of NK012 (i.e., SN-38–releasing polymeric micelles) against human cancer xenografts compared with CPT-11. Here, we investigated the advantages of NK012 over CPT-11 treatment in mouse models of gastric cancer with peritoneal dissemination. NK012 or CPT-11 was i.v. administered thrice every 4 days at their respective maximum tolerable doses (NK012, 30 mg/kg/day; CPT-11, 67 mg/kg/day) to mice receiving orthotopic transplants of gastric cancer cell lines (44As3Luc and 58As1mLuc) transfected with the luciferase gene (n = 5). Antitumor effect was evaluated using the photon counting technique. SN-38 concentration in gastric tumors and peritoneal nodules was examined by high-performance liquid chromatography (HPLC) 1, 24, and 72 hours after each drug injection. NK012 or CPT-11 distribution in these tumors was evaluated using a fluorescence microscope on the same schedule. In both models, the antitumor activity of NK012 was superior to that of CPT-11. High concentrations of SN-38 released from NK012 were detected in gastric tumors and peritoneal nodules up to 72 hours by HPLC. Only a slight conversion from CPT-11 to SN-38 was observed from 1 to 24 hours. Fluorescence originating from NK012 was detected up to 72 hours, whereas that from CPT-11 disappeared until 24 hours. NK012 also showed antitumor activity against peritoneal nodules. Thus, NK012 showing enhanced distribution with prolonged SN-38 release may be ideal for cancer treatment because the antitumor activity of SN-38 is time dependent. [Cancer Res 2008;68(22):9318–22]

Introduction

Gastric cancer is the second most common cause of death from cancer in the world. The survival rate has remained low in patients with advanced gastric cancer, with a median survival rate of 13 months having been recently reported in a phase III trial, which has been the best outcome thus far (1). Patients with gastric cancer with scirrhous type stroma particularly showed poor prognosis even after curative resection, as well as highly progressed peritoneal dissemination (2). Because peritoneal dissemination causes several refractory symptoms such as massive ascites, intestinal obstruction, hydronephrosis, and obstructive jaundice, the quality of life of patients at the end stage of cancer is severely impaired.

Poor delivery of anticancer drugs to peritoneal metastatic cells may be one of the reasons for the poor prognosis of patients with peritoneal dissemination (3). In peritoneal nodules, the distribution and eventual diffusion of drugs to cancer cells tend to be impeded because of several obstacles such as severe fibrosis and high interstitial pressure (4, 5). On the other hand, angiogenesis was reported to be an essential factor in the development of peritoneal metastasis, and the high expression level of vascular endothelial growth factor (VEGF) in primary gastric tumors or ascitic fluid, which can enhance tumor vascular permeability, was found to be directly associated with the development of ascites and peritoneal dissemination (6–10). In addition, several factors such as kinins and nitric oxide are involved in tumor vascular permeability (11–13). Polymer-conjugated drugs and nanoparticles categorized under drug delivery system agents are favorably extravasated from the vessels into the interstitium of tumors due to the enhanced permeability and retention effect (EPR effect; refs. 14, 15). The EPR effect is based on the following pathophysiologic characteristics of solid tumor tissues: hypervascularity, incomplete vascular architecture, secretion of vascular permeability factors stimulating extravasation within cancer tissue, and absence of effective lymphatic drainage from the tumors that impedes the efficient clearance of macromolecules accumulated in solid tumor tissues. Moreover, macromolecules cannot freely leak out from normal vessels, and thus, the side effects of an anticancer agent can be reduced. Very recently, we have shown that NK012 (i.e., SN-38–releasing polymeric micelles) exerted superior antitumor activity and less toxicity than CPT-11 (15–17). In a series of studies, we showed that NK012 markedly enhanced the antitumor activity of SN-38, particularly against highly VEGF-secreting SBC-3/VEGF tumors compared with SBC-3/Neo tumors. On the other hand, it is conceivable that satisfactory drug delivery cannot be achieved in less-vascularized and highly fibrotic tumors, particularly for macromolecules. However, we observed that NK012 showed a strong antitumor activity even in the xenograft of Capan1 cells, which are pancreatic cancer cells with abundant stromal tissue, compared with CPT-11. This result suggests that NK012 can selectively accumulate in both hypervascular and hypovascular tumors with high interstitial pressure, and then induce sustained

Requests for reprints: Yasuhiro Matsumura, Investigative Treatment Division, Research Center for Innovative Oncology, National Cancer Center Hospital East, 6-5-1 Kashiwanoha, Kashiwa, Chiba 277-8577, Japan. Phone: 81-4-7134-6857; Fax: 81-4-7134-6866; E-mail: yhmatsum@east.ncc.go.jp.

doi:10.1158/0008-5472.CAN-08-2822

release of SN-38, followed by SN-38 distribution throughout the entire tumor tissues. In the present study, we evaluated the antitumor activity of NK012 against peritoneal tumor dissemination compared with that of CPT-11 using mouse models orthotopically transplanted with scirrhous gastric cancer cells, as well as against spontaneously progressing peritoneal dissemination (18, 19).

Materials and Methods

Cell cultures. 44As3 and 58Aslm were previously reported as human signet-ring cell gastric cancer cell lines that spontaneously metastasize to the peritoneal cavity and produce large volumes of bloody ascites after orthotopic implantion in the gastric wall (18–21). Here, 44As3 and 58Aslm cells were transfected with a complex of 4 μg of pEGF-PLuc plasmid DNA (Clontech) and 24 μL of GeneJammer reagent (Stratagene; Cloning Systems) in accordance with the manufacturer's instructions. Stable transfectants were selected in geneticin (400 μg/mL; Invitrogen), and bioluminescence was used to screen transfected clones for luciferase gene expression using the IVIS system (Xenogen). Clones expressing the luciferase gene were named 44As3Luc and 58AslmLuc. 44As3Luc and 58AslmLuc cells were maintained in RPMI 1640 supplemented with 10% FCS (Sigma), 100 IU/mL penicillin G sodium, and 100 mg/mL streptomycin sulfate (Immuno-Biological Laboratories) in a humidified atmosphere containing 5% CO_2 at 37°C.

Orthotopic models *in vivo*. Six-week-old female BALB/c *nu/nu* mice were purchased from CLEA Japan, Inc., and maintained under specific pathogen-free conditions and provided with sterile food, water, and cages. Ambient light was controlled to provide regular cycles of 12 h of light and 12 h of darkness. A total of 1×10^6 cells of 44As3Luc or 58AslLuc were inoculated into the gastric wall of each mouse after laparotomy, as described previously (18–21). *In vivo* photon counting analysis was conducted on a cryogenically cooled IVIS system using Living Image acquisition and analysis software (Xenogen). All animal procedures were performed in compliance with the Guidelines for the Care and Use of Experimental Animals established by the Committee for Animal Experimentation of the National Cancer Center; these guidelines conform to the ethical standards required by law and also comply with the guidelines for the use of experimental animals in Japan.

Drugs. NK012 was prepared by Nippon Kayaku Co., Ltd. (15). CPT-11 was purchased from Yakult Honsha Co., Ltd.

***In vivo* growth inhibition assay.** After inoculation of 44As3Luc or 58AslmLuc cells into the gastric wall (day 0), mice were randomly divided into test groups consisting of 5 mice per group. 44As3Luc mice were i.v. administered the maximum tolerated dose (MTD) of the 2 drugs via the tail vein on days 20, 24, and 28 as previously reported, that is, at 66.7 mg/kg/d for CPT-11 and 30 mg/kg/d for NK012 (15). 58AslmLuc mice were given the drugs in the same manner on days 18, 22, and 26. Photon counting analysis and body weight were measured twice a week. "Visible ascites," which was evident a few days before death in this mouse model, was used as a surrogate for survival time in consideration of animal welfare. Mice were euthanized when ascites became visible, and colonization of gastric wall by cancer cells and metastasis to the peritoneal cavity were confirmed in all the euthanized mice. Differences in relative photon counts between the treatment groups at day 42 in 44As3Luc mice and at day 81 in 58AslmLuc mice were analyzed using the unpaired *t* test.

Assay of free SN-38 in tissues. We next analyzed the biodistributions of NK012 and CPT-11 to orthotopic gastric tumors and peritoneal nodules. Twenty-six days after the inoculation of 44As3Luc cells into the gastric wall of mice, NK012 (30 mg/kg) or CPT-11 (66.7 mg/kg) was administered via the tail vein. Under anesthesia, orthotopic gastric tumor and peritoneal nodule samples were excised 1, 24, and 72 hours after injection.

Measurements of tissue concentration of free SN-38 by high-performance liquid chromatography. Samples were rinsed with physiologic saline, mixed with 0.1 mol/L glycine-HCl buffer (pH 3.0)/methanol at 5 w/w%, and then homogenized. To analyze the concentration of free SN-38, 100 μL of the tumor samples were mixed with 20 μL of 1 mmol/L phosphoric acid/methanol (1:1) and 40 μL of ultrapure water, and camptothecin (CPT) was used as the internal standard (10 ng/mL for free SN-38). The samples were vortexed vigorously for 10 s, and then filtered

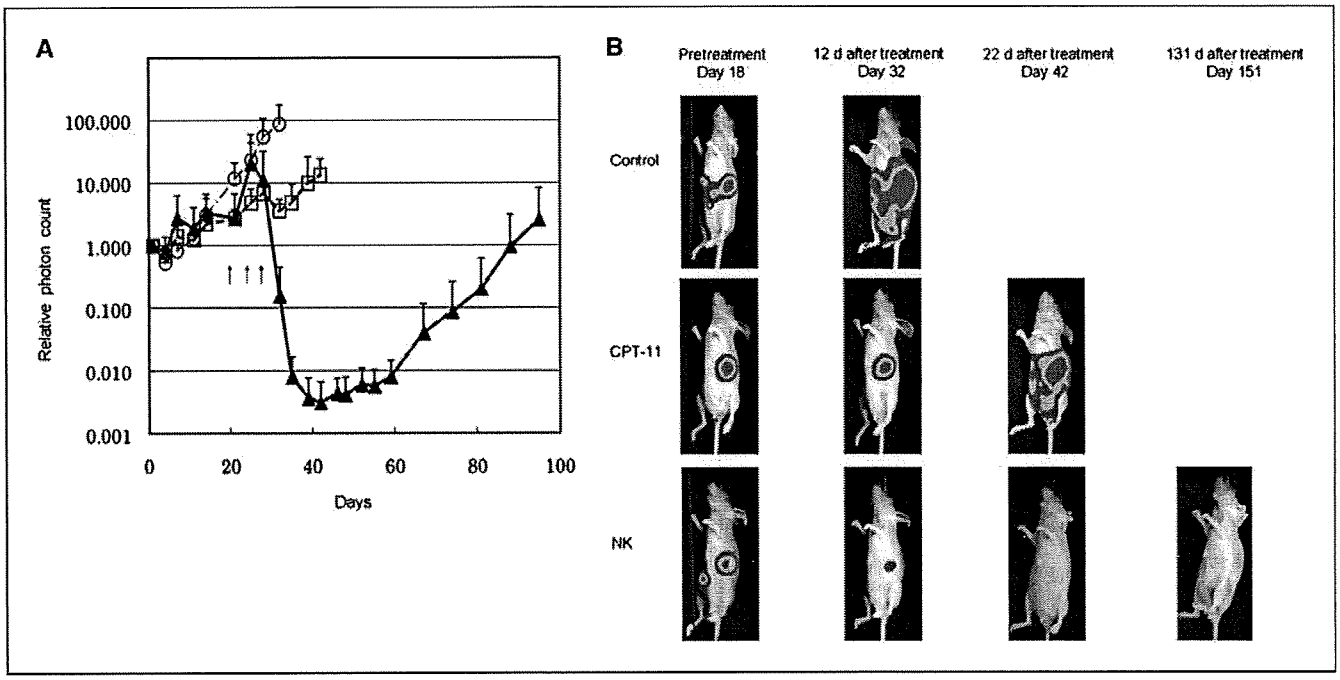

Figure 1. Effects of NK012 and CPT-11 in 44As3Luc mouse models. *A*, antitumor activity of NK012 or CPT-11 was evaluated by counting the number of photons using the IVIS system (*points*, mean; *bars*, SD; *arrows*, drug injections). Antitumor effect of each regimen on days 20, 24, and 28. (○), control; (□), CPT-11 (66.7 mg/kg/d, ×3); and (▲), NK012 (30 mg/kg/d, ×3) in 44As3Luc mouse model. *B*, images of 44As3Luc mouse model administered NK012 taken using the IVIS system on days 18, 32, 42, and 151 after inoculation of 44As3Luc cells. Data were derived from the same mice as those used in the present study.

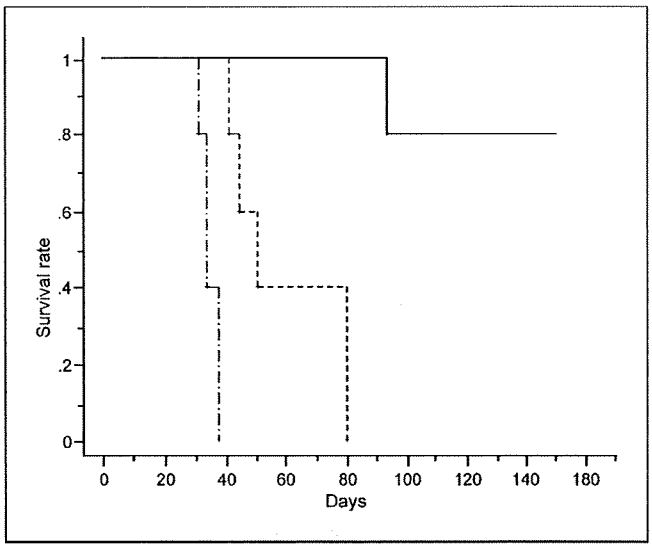

Figure 2. Survival curves of 44As3Luc mouse models. Survival curves of 44As3Luc mouse model in each regimen on days 20, 24, and 28. (–·–·–), control; (– – –), CPT-11 given at 66.7 mg/kg/d ×3; and (——), NK012 given at 30 mg/kg/d ×3.

through Ultrafree-MC Centrifugal Filter Devices with a cutoff molecular diameter of 0.45 μm (Millipore Co.). Reversed-phase high-performance liquid chromatography (HPLC) was conducted at 35°C on a Mightysil RP-18 GP column (150 × 4.6 mm; Kanto Chemical Co., Inc.). Fifty microliters of a sample were injected into an Alliance Water 2795 HPLC system (Waters) equipped with a Waters 2475 multi λ fluorescence detector. Fluorescence originating from SN-38 was detected at 540 nm with an excitation wavelength of 365 nm. The mobile phase was a mixture of 100 mmol/l ammonium acetate (pH 4.2) and methanol [11:9 (v/v)], and the flow rate was 1.0 mL/min. The content of SN-38 was calculated by measuring the relevant peak area and calibrating against the corresponding peak area derived from the CPT internal standard. Peak data were recorded using a chromatography management system (MassLynx v4.0; Waters).

Visualization of distribution of NK012 and CPT-11 by fluorescence microscopy. Mice were given fluorescein *Lycopersicon esculentum* lectin (100 μL per mouse; Vector Laboratories) to visualize tumor vasculature in the samples 5 min before anesthesia. The samples were then excised and embedded in an optimal cutting temperature compound (Sakura Finetechnochemical Co., Ltd.) and frozen at −80°C. Six-μm-thick tumor sections were then prepared using a cryostatic microtome, Tissue-Tek Cryo3 (Sakura Finetechnochemical Co., Ltd.). Frozen sections were examined under a fluorescence microscope, BIOZERO (KEYENCE), at an excitation wavelength of 377 nm and an emission wavelength 447 nm to evaluate the distribution of NK012 and CPT-11. Both drugs could be detected under the same fluorescence conditions because formulations containing SN-38 bound via ester bonds possess a particular fluorescence.

Statistical analyses. Data were expressed as mean ± SD. Data were analyzed using the Student's *t* test when groups showed equal variances (*F* test), or the Welch's test when they showed unequal variances (*F* test). *P* value of <0.05 was considered as significant. All statistical tests were two sided.

Results

Antitumor activities of NK012 and CPT-11. Comparison of the relative photon counts on day 42 in the 44As3Luc mouse model revealed significant differences in counts between mice given with NK012 and those given with CPT-11 ($P = 0.0282$; Fig. 1*A* and *B*). Similar result was obtained in the experiment with 58As gastric tumor (data not shown). The survival rates on day 150 in the 44As3Luc mouse model were 80% and 0% for the NK012 group and CPT-11 group, respectively (Fig. 2). Similar result was obtained in the experiment with 58As gastric tumor (data not shown). No marked toxic effects in terms of body weight changes were observed in any groups for any mouse models (data not shown). Only 1 mouse in the CPT-11 group of 44As1 mouse models showed diarrhea for 3 d, and any other clinical symptoms were not observed.

Tissue concentrations of free SN-38 after administration of NK012 and CPT-11. We examined the concentration-time profile of free SN-38 in orthotopic gastric tumors and peritoneal nodules in the 44As3Luc mouse model after the administration of NK012 and CPT-11 (Fig. 3*A* and *B*). Either orthotopic gastric tumors or peritoneal nodules exhibited the highest concentration of free SN-38 24 hours after NK012 administration, and 1 hour after CPT-11 administration. The highest concentrations of free SN-38 in the NK012 group were much higher than those in the CPT-11 group in either orthotopic gastric tumors or peritoneal nodules. The concentrations of free SN-38 released from NK012 in orthotopic gastric tumors were higher than those in peritoneal nodules.

Tumor tissue distribution of NK012 and CPT-11 as determined by fluorescence microscopy. Results showed that NK012 accumulation in either orthotopic gastric tumors or peritoneal nodules had been maintained from 1 hour to 72 hours after injection (Fig. 4*A*). On the other hand, CPT-11 showed maximum accumulation in either orthotopic gastric tumors or peritoneal nodules 1 hour after injection and disappeared within 24 hours (Fig. 4*B*).

Discussion

The main purpose of this study was to clarify the advantages of NK012 over CPT-11 as treatment against peritoneal metastasis spontaneously disseminated from orthotopically transplanted scirrhous gastric cancer cells in mouse models. We showed that NK012 exerted more potent antitumor activity in the mouse models used than CPT-11. Therefore, NK012 is considered promising in terms of providing clinical benefit to patients with gastric cancer showing progressing peritoneal dissemination.

CPT-11 is converted to SN-38, a biologically active and water-insoluble metabolite of CPT-11, by carboxylesterases (CE) in the liver and tumors. However, only 2% to 8% of administered CPT-11 is converted by CE in the liver and tumors to the active form SN-38 (22, 23). The conversion of CPT-11 to SN-38 also depends on genetic interindividual variability of the activity of CE (24). Thus, the direct use of SN-38 might be of great advantage and is attractive for cancer treatment. We have recently shown that NK012 (i.e., SN-38–releasing polymeric micelles) exerted superior antitumor activity and less toxicity than CPT-11 (15–17). The mean particle size of NK012 is 20 nm in diameter. NK012 can release SN-38 under neutral conditions even in the absence of CE because SN-38, which is bound to the blockcopolymer by phenolic ester binding, is stable under acidic conditions but relatively labile under neutral and mild alkaline conditions. The release rate of SN-38 from NK012 under physiologic conditions is quite high, that is, >70% of SN-38 is gradually released within 48 hours.

In this study, we used mouse models with orthotopically transplanted human scirrhous gastric cancer cells showing spontaneously progressing peritoneal dissemination, which we

reported previously (18, 19, 21). These models can imitate more realistically the progressing mode of human peritoneal dissemination of gastric cancer than conventional experimental models directly transplanted with cancer cells i.p. Moreover, our models enabled us to quantitatively evaluate drug antitumor effect even against peritoneal dissemination without having to sacrifice the animal and perform autopsy through the use of gastric cancer cells transfected with the luciferase gene and by applying photon counting analysis, having already verified the significant correlation between tumor volume and photon counts in a previous report (19).

For *in vivo* growth inhibition assay, drug administration was started on day 18 or 20 after cell inoculation into the gastric wall, when small peritoneal metastatic nodules and a small degree of ascites had appeared. The present results showed that NK012 had more potent antitumor activity than CPT-11 in the mouse models tested, suggesting its effectiveness against peritoneal dissemination of gastric cancer in the clinical setting.

In the pharmacologic evaluation, we could confirm the more enhanced distribution of NK012 than CPT-11 to not only orthotopic gastric tumors but also peritoneal nodules by quantifying SN-38 concentration in the tumors and visualization of fluorescence originating from NK012 or CPT-11 distributed in the tumors. Because CPT-11 or SN-38 has been reported to possess time-dependent growth-inhibitory activity against tumor cells, this prolonged retention of NK012 in the tumors and the sustained release of free SN-38 from NK012 may be responsible for its more potent antitumor activity observed in the present study (25). On the other hand, CPT-11 disappeared from the tumors before exerting sufficient antitumor activity. For both drugs, however, the concentrations of SN-38 in orthotopic gastric tumors were higher than those

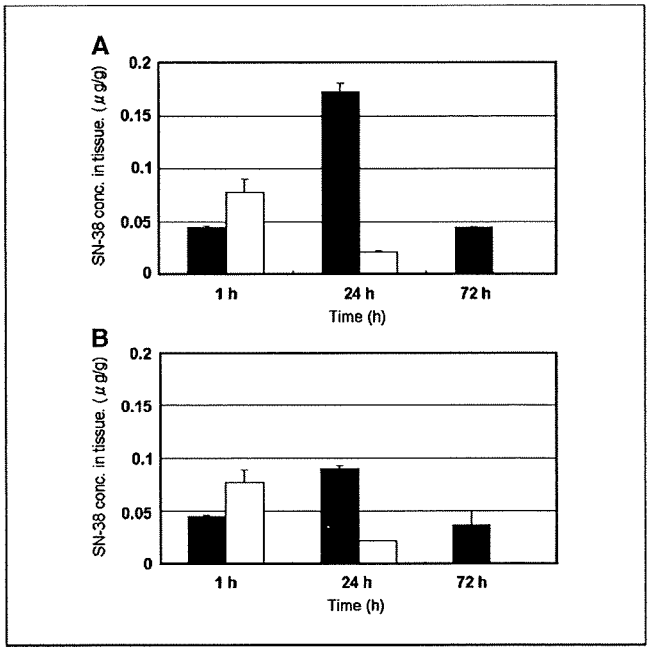

Figure 3. Concentration-time profile of free SN-38. NK012 (30 mg/kg) or CPT-11 (66.7 mg/kg) was injected 26 d after implantation of 44As3Luc gastric cancer cells (*columns*, mean; *bars*, SD). *A*, concentration (*conc.*) of free SN-38 in orthotopic gastric tumor tissue of 44As3Luc mouse model after administration of NK012 (*black column*) and CPT-11 (*white column*). *B*, concentration of free SN-38 in peritoneal nodules of 44As3Luc mouse model after administration of NK012 (*black column*) and CPT-11 (*white column*).

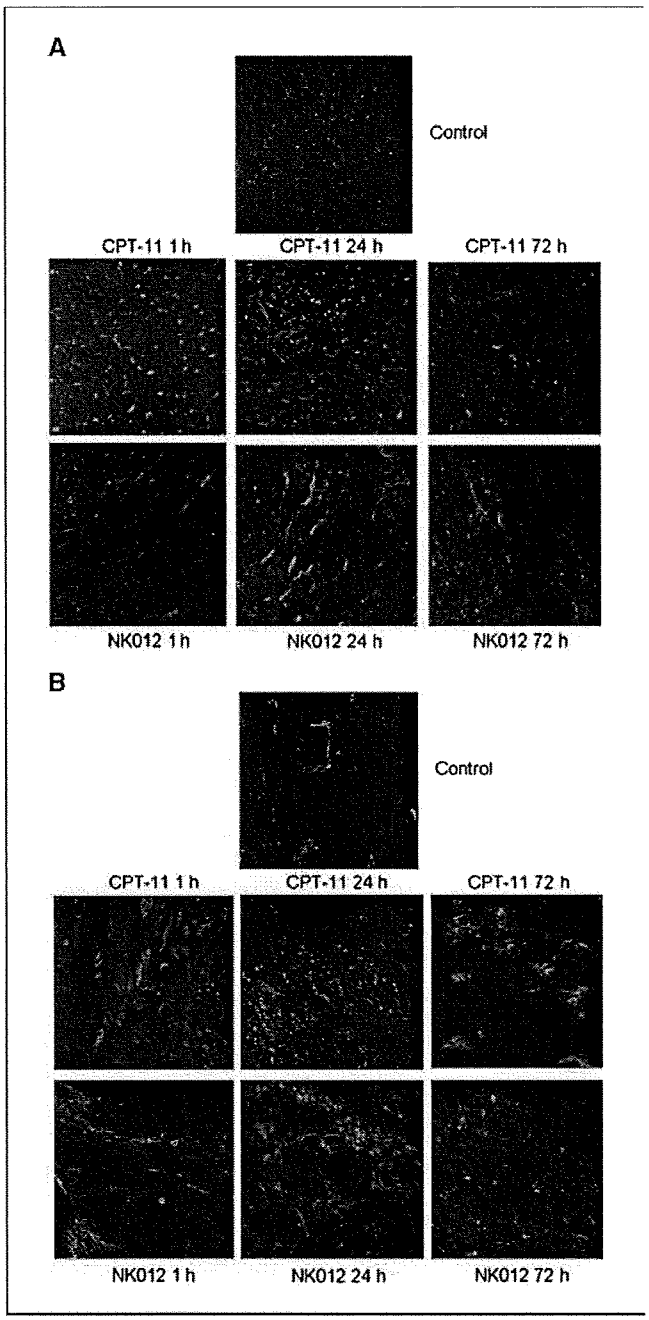

Figure 4. Tissue distribution of NK012 and CPT-11 as determined by fluorescence microscopy. Orthotopic gastric tumors or peritoneal nodules of 44As3Luc mouse model were excised 1, 24, and 72 h after i.v. injection of NK012 (30 mg/kg) or CPT-11 (66.7 mg/kg). Each mouse was i.v. administered with fluorescein-labeled *Lycopersicon esculentum* lectin just before being sacrificed to detect tumor blood vessels. Frozen sections were examined under a fluorescence microscope at an excitation wavelength of 377 nm and an emission wavelength of 447 nm. The same fluorescence condition can be applied for visualizing NK012 and CPT-11 fluorescence. Free SN-38 cannot be detected under this fluorescence condition. *A*, distribution of NK012 or CPT-11 in orthotopic gastric tumors (×100). *B*, distribution of NK012 or CPT-11 in peritoneal nodules (×100).

in peritoneal nodules. This is consistent with previous reports stating the poor delivery of anticancer drugs to peritoneal metastatic cells probably because of some obstacles such as abundant interstitium or high interstitial pressure. To date, we reported that NK012 can

more selectively accumulate and retain longer in various tumor xenografts transplanted s.c. compared with CPT-11 (15–17). In the present study, we succeeded in demonstrating higher accumulation and longer retention of NK012 compared with CPT-11 in orthotopic and peritoneal disseminated gastric cancer model that is closer to human gastric cancer in clinics.

Peritoneal dissemination sometimes causes intestinal obstruction, which enhances the enterohepatic circulation of SN-38 after direct damage to the small intestine, and makes the use of CPT-11 difficult (26, 27). In the present study, no mouse in the NK012 group developed diarrhea. The dose-limiting toxic effects of CPT-11 seem to be neutropenia and diarrhea. In our previous data, however, there was no significant difference in the level of SN-38 in the small intestine between mice treated with NK012 and mice treated with CPT-11 despite the higher plasma area under the concentration of NK012 than CPT-11 (15). Moreover, no serious diarrhea has been reported even at the MTD dose in two phase I clinical trials against advanced solid tumors in Japan and the US (28, 29).

In conclusion, we showed that NK012 exerts significantly more potent antitumor activity against peritoneal dissemination of scirrhous gastric cancer cells than CPT-11, indicating the possibility of the clinical evaluation of this drug in patients with disseminated grastic cancer.

Disclosure of Potential Conflicts of Interest

No potential conflicts of interest were disclosed.

Acknowledgments

Received 7/23/2008; revised 9/2/2008; accepted 9/16/2008.

Grant support: Third Term Comprehensive Contorol Research for Cancer from the Ministry of Health, Labor and Welfare of Japan (Y. Matsumura) and a Grant-in-Aid for Scientific Research on Priority Areas from the Ministry of Education, Culture, Sports, Science and Technology (Y. Matsumura).

The costs of publication of this article were defrayed in part by the payment of page charges. This article must therefore be hereby marked *advertisement* in accordance with 18 U.S.C. Section 1734 solely to indicate this fact.

References

1. Koizumi W, Narahara H, Hara T, et al. S-1 plus cisplatin versus S-1 alone for first-line treatment of advanced gastric cancer (SPIRITS trial): a phase III trial. Lancet Oncol 2008;9:215–21.
2. Maehara Y, Moriguchi S, Orita H, et al. Lower survival rate for patients with carcinoma of the stomach of Borrmann type IV after gastric resection. Surg Gynecol Obstet 1992;175:13–6.
3. Yonemura Y. Mechanisms of drug resistance in gastric cancer. In: Yonemura Y, editor. Contemporary Approaches Toward Cure of Gastric Cancer. Kanazawa: Maeda Shoten Co. Ltd.; 1996. p. 87–91.
4. Yashiro M, Chung YS, Nishimura S, Inoue T, Sowa M. Fibrosis in the peritoneum induced by scirrhous gastric cancer cells may act as "soil" for peritoneal dissemination. Cancer 1996;77:1668–75.
5. Jain RK. Barriers to drug delivery in solid tumors. Sci Am 1994;271:58–65.
6. Senger DR, Galli SJ, Dvorak AM, Perruzzi CA, Harvey VS, Dvorak HF. Tumor cells secrete a vascular permeability factor that promotes accumulation of ascites fluid. Science 1983;219:983–5.
7. Dvorak HF, Brown LF, Detmar M, Dvorak AM. Vascular permeability factor/vascular endothelial growth factor, microvascular hyperpermeability, and angiogenesis. Am J Pathol 1995;146:1029–39.
8. Nagy JA, Masse EM, Herzberg KT, et al. Pathogenesis of ascites tumor growth: vascular permeability factor, vascular hyperpermeability, and ascites fluid accumulation. Cancer Res 1995;55:360–8.
9. Boocock CA, Charnock-Jones DS, Sharkey AM, et al. Expression of vascular endothelial growth factor and its receptors flt and KDR in ovarian carcinoma. J Natl Cancer Inst 1995;87:506–16.
10. Aoyagi K, Kouhuji K, Yano S, et al. VEGF significance in peritoneal recurrence from gastric cancer. Gastric Cancer 2005;8:155–63.
11. Maeda H, Matsumura Y, Kato H. Purification and identification of [hydroxyprolyl3]bradykinin in ascitic fluid from a patient with gastric cancer. J Biol Chem 1988;263:16051–4.
12. Matusmura Y, Maruo K, Kimura M, Yamamoto T, Konno T, Maeda H. Kinin-generating cascade in advanced cancer patients and *in vitro* study. Jpn J Cancer Res 1991;82:732–41.
13. Wu J, Akaike T, Hayashida K, et al. Identification of bradykinin receptors in clinical cancer specimens and murine tumor tissues. Int J Cancer 2002;98:29–35.
14. Matsumura Y, Maeda H. A new concept for macromolecular therapeutics in cancer chemotherapy: mechanism of tumoritropic accumulation of proteins and the antitumor agent smancs. Cancer Res 1986;46:6387–92.
15. Koizumi F, Kitagawa M, Negishi T, et al. Novel SN-38-incorporating polymeric micelles, NK012, eradicate vascular endothelial growth factor-secreting bulky tumors. Cancer Res 2006;66:10048–56.
16. Nakajima TE, Yasunaga M, Kano Y, et al. Synergistic antitumor activity of the novel SN-38-incorporating polymeric micelles, NK012, combined with 5-fluorouracil in a mouse model of colorectal cancer, as compared with that of irinotecan plus 5-fluorouracil. Int J Cancer 2008;122:2148–53.
17. Saito Y, Yasunaga M, Kuroda J, Koga Y, Matsumura Y. Enhanced distribution of NK012, a polymeric micelle-encapsulated SN-38, and sustained release of SN-38 within tumors can beat a hypovascular tumor. Cancer Sci 2008;99:1258–64.
18. Yanagihara K, Takigahira M, Tanaka H, et al. Development and biological analysis of peritoneal metastasis mouse models for human scirrhous stomach cancer. Cancer Sci 2005;96:323–32.
19. Yanagihara K, Takigahira M, Takeshita F, et al. A photon counting technique for quantitatively evaluating progression of peritoneal tumor dissemination. Cancer Res 2006;66:7532–9.
20. Yanagihara K, Tanaka H, Takigahira M, et al. Establishment of two cell lines from human gastric scirrhous carcinoma that possess the potential to metastasize spontaneously in nude mice. Cancer Sci 2004;95:575–82.
21. Arao T, Yanagihara K, Takigahira M, et al. ZD6474 inhibits tumor growth and intraperitoneal dissemination in a highly metastatic orthotopic gastric cancer model. Int J Cancer 2006;118:483–9.
22. Slatter JG, Schaaf LJ, Sams JP, et al. Pharmacokinetics, metabolism, and excretion of irinotecan (CPT-11) following I.V. infusion of [(14)C]CPT-11 in cancer patients. Drug Metab Dispos 2000;28:423–33.
23. Rothenberg ML, Kuhn JG, Burris HA III, et al. Phase I and pharmacokinetic trial of weekly CPT-11. J Clin Oncol 1993;11:2194–204.
24. Guichard S, Terret C, Hennebelle I, et al. CPT-11 converting carboxylesterase and topoisomerase activities in tumour and normal colon and liver tissues. Br J Cancer 1999;80:364–70.
25. Kawato Y, Aonuma M, Hirota Y, Kuga H, Sato K. Intracellular roles of SN-38, a metabolite of the camptothecin derivative CPT-11, in the antitumor effect of CPT-11. Cancer Res 1991;51:4187–91.
26. Araki E, Ishikawa M, Iigo M, Koide T, Itabashi M, Hoshi A. Relationship between development of diarrhea and the concentration of SN-38, an active metabolite of CPT-11, in the intestine and the blood plasma of athymic mice following intraperitoneal administration of CPT-11. Jpn J Cancer Res 1993;84:697–702.
27. Atsumi R, Suzuki W, Hakusui H. Identification of the metabolites of irinotecan, a new derivative of camptothecin, in rat bile and its biliary excretion. Xenobiotica 1991;21:1159–69.
28. Kato K, Hamaguchi T, Shirao K, et al. Interim analysis of phase I study of NK012, polymer micelle SN-38, in patients with advanced cancer. Proc Am Soc Clin Oncol GI 2008 (Abs #485).
29. Burris HA III, Infante JR, Spigel DR, et al. A phase I dose-escalation study of NK012. Proc Am Soc Clin Oncol 2008 (Abs #2358).

Int. J. Cancer: **122,** 2148–2153 (2008)

Synergistic antitumor activity of the novel SN-38-incorporating polymeric micelles, NK012, combined with 5-fluorouracil in a mouse model of colorectal cancer, as compared with that of irinotecan plus 5-fluorouracil

Takako Eguchi Nakajima[1,2], Masahiro Yasunaga[2], Yasuhiko Kano[3], Fumiaki Koizumi[4], Ken Kato[1], Tetsuya Hamaguchi[1], Yasuhide Yamada[1], Kuniaki Shirao[1], Yasuhiro Shimada[1] and Yasuhiro Matsumura[2]*

[1]*Gastrointestinal Oncology Division, National Cancer Center Hospital, Tokyo, Japan*
[2]*Investigative Treatment Division, Research Center for Innovative Oncology, National Cancer Center Hospital East, Kashiwa, Chiba, Japan*
[3]*Hematology Oncology, Tochigi Cancer Center, Tochigi, Japan*
[4]*Shien Lab Medical Oncology Division, National Cancer Center Hospital, Tokyo, Japan*

The authors reported in a previous study that NK012, a 7-ethyl-10-hydroxy-camptothecin (SN-38)-releasing nano-system, exhibited high antitumor activity against human colorectal cancer xenografts. This study was conducted to investigate the advantages of NK012 over irinotecan hydrochloride (CPT-11) administered in combination with 5-fluorouracil (5FU). The cytotoxic effects of NK012 or SN-38 (an active metabolite of CPT-11) administered in combination with 5FU was evaluated *in vitro* in the human colorectal cancer cell line HT-29 by the combination index method. The effects of the same drug combinations was also evaluated *in vivo* using mice bearing HT-29 and HCT-116 cells. All the drugs were administered i.v. 3 times a week; NK012 (10 mg/kg) or CPT11 (50 mg/kg) was given 24 hr before 5FU (50 mg/kg). Cell cycle analysis in the HT-29 tumors administered NK012 or CPT-11 *in vivo* was performed by flow cytometry. NK012 exerted more synergistic activity with 5FU compared to SN-38. The therapeutic effect of NK012/5FU was significantly superior to that of CPT-11/5FU against HT-29 tumors ($p = 0.0004$), whereas no significant difference in the antitumor effect against HCT-116 tumors was observed between the 2-drug combinations ($p = 0.2230$). Cell-cycle analysis showed that both NK012 and CPT-11 tend to cause accumulation of cells in the S phase, although this effect was more pronounced and maintained for a more prolonged period with NK012 than with CPT-11. Optimal therapeutic synergy was observed between NK012 and 5FU, therefore, this regimen is considered to hold promise of clinical benefit, especially for patients with colorectal cancer.

Key words: NK012; SN-38; 5-fluorouracil; drug delivery system; colorectal cancer

The 5-year survival rates of colorectal cancer (CRC) have improved remarkably over the last 10 years, accounted for in large part by the extensively investigated agents after 5-fluorouracil (5FU). Irinoetcan hydrochloride (CPT-11), a water-soluble, semi-synthetic derivative of camptothecin, is one such agent that has been shown to be highly effective, and currently represents a key-drug in first- and second-line treatment regimens for CRC. CPT-11 monotherapy, however, has not been shown to yield superior efficacy, including in terms of the median survival time, to bolus 5FU/leucovorin (LV) alone.[1] In 2 Phase III trials, the addition of CPT-11 to bolus or infusional 5FU/LV regimens clearly yielded greater efficacy than administration of 5FU/LV alone, with a doubling of the tumor response rate and prolongation of the median survival time by 2–3 months.[1,2]

CPT-11 is converted to 7-ethyl-10-hydroxy-camptothecin (SN-38), a biologically active and water-insoluble metabolite of CPT-11, by carboxylesterases in the liver and the tumor. SN-38 has been demonstrated to exhibit up to a 1,000-fold more potent cytotoxic activity than CPT-11 against various cancer cells *in vitro*.[3] The metabolic conversion rate is, however, very low, with only <10% of the original volume of CPT-11 being metabolized to SN-38[4,5]; conversion of CPT-11 to SN-38 also depends on genetic interindividual variability of the activity of carboxylesterases.[6] Direct use of SN-38 itself for clinical cancer treatment must be shown to be identical in terms of both efficacy and toxicity.

Some drugs incorporated in drug delivery systems (DDS), such as Abraxane and Doxil, are already in clinical use.[7,8] The clinical benefits of DDS are based on their EPR effect.[9] The EPR effect is based on the pathophysiological characteristics of solid tumor tissues: hypervascularity, incomplete vascular architecture, secretion of vascular permeability factors stimulating extravasation within cancer tissue, and absence of effective lymphatic drainage from the tumors that impedes the efficient clearance of macromolecules accumulated in solid tumor tissues. Several types of DDS can be used for incorporation of a drug. A liposome-based formulation of SN-38 (LE-SN38) has been developed, and a clinical trial to assess its efficacy is now under way.[10,11]

Recently, we demonstrated that NK012, novel SN-38-incorporating polymeric micelles, exerted superior antitumor activity and less toxicity than CPT-11.[12] NK012 is characterized by a smaller size of the particles than LE-SN38; the mean particle diameter of NK012 is 20 nm. NK012 can release SN-38 under neutral conditions even in the absence of a hydrolytic enzyme, because the bond between SN-38 and the block copolymer is a phenol ester bond, which is stable under acidic conditions and labile under mild alkaline conditions. The release rate of SN-38 from NK012 under physiological conditions is quite high; more than 70% of SN-38 is released within 48 hr. We speculated that the use of NK012, in place of CPT-11, in combination with 5FU may yield superior results in the treatment of CRC. In the present study, we evaluated the antitumor activity of NK012 administered in combination with 5FU as compared to that of CPT-11 administered in combination with 5FU against CRC in an experimental model.

Material and methods

Cells and animals

The human colorectal cancer cell lines used, namely, HT-29 and HCT-116, were purchased from the American Type Culture Collection (Rockville, MD). The HT-29 cells and HCT-116 cells were maintained in RPMI 1640 supplemented with 10% fetal bovine serum (Cell Culture Technologies, Gaggenau-Hoerden, Germany), penicillin, streptomycin, and amphotericin B (100 units/mL, 100 μg/mL, and 25 μg/mL, respectively; Sigma, St. Louis, MO) in a humidified atmosphere containing 5% CO_2 at 37°C.

BALB/c *nu/nu* mice were purchased from SLC Japan (Shizuoka, Japan). Six-week-old mice were subcutaneously (s.c.)

***Correspondence to:** Investigative Treatment Division, Research Center for Innovative Oncology, National Cancer Center Hospital East, 6-5-1 Kashiwanoha, Kashiwa, Chiba 277-8577, Japan. Fax: +81-4-7134-6866.
E-mail: yhmatsum@east.ncc.go.jp
Received 2 September 2007; Accepted after revision 20 November 2007
DOI 10.1002/ijc.23381
Published online 14 January 2008 in Wiley InterScience (www.interscience.wiley.com).